Laser Welding of Dissimilar Materials: Mathematical & Numerical Modelling

Submitted by

SAURAV KUMAR GHOSH

Examination Roll No – M4LST23003

Registration No – 160420 of 2021-22

A thesis submitted towards partial fulfillment of the requirements for the degree of

Master of Technology in Laser Technology

A course affiliated to Faculty of Engineering and Technology

and offered by

Faculty Council of Interdisciplinary Studies, Law and Management,
Jadavpur University

Under the Guidance of

Dr. Nilkanta Barman
Professor
Department of Mechanical Engineering
Jadavpur University, Kolkata – 700032

School of Laser Science and Engineering

Faculty Council of Interdisciplinary Studies, Law and management

Jadavpur University

Kolkata-700032

FACULTY COUNCIL OF INTERDISCIPLINARY STUDIES LAW

& MANAGEMENT

JADAVPUR UNIVERSITY

DECLARATION OF ORIGINALITY AND COMPLIANCE OF ACADEMIC ETHICS

The author hereby declares that this thesis contains original research work by the undersigned candidate, as part of his **Master of Technology in Laser Technology** studies during academic session 2021-2023.

All information in this document has been obtained and presented in accordance with academic rules and ethical conduct.

The author also declares that as required by this rules and conduct, the author has fully cited and referred all material and results that are not original to this work.

Name- Saurav Kumar Ghosh

Examination Roll No.- M4LST23003

Thesis Title: Laser Welding of Dissimilar Materials: Mathematical & Numerical Modelling

Signature:

Date:

M.TECH IN LASER SCIENCE AND TECHNOLOGY

Course affiliated to

FACULTY OF ENGINEERING & TECHNOLGY

Under

FACULTY COUNCIL OF INTERDISCIPLINARY STUDIES LAW & MANAGEMENT

JADAVPUR UNIVERSITY

Certificate of Recommendation

We hereby recommend that the thesis, entitled as "**Laser Welding of Dissimilar Materials: Mathematical & Numerical Modelling**", prepared by Mr. Saurav Kumar Ghosh (Registration No – 160420 of 2021- 2022) under our guidance, be accepted in partial fulfillment of the requirement for the degree of Master of Technology in Laser Science and Technology from the Department of School of Laser Science And Engineering of Jadavpur University.

…….

Adviser,

Dr. Nilkanta Barman

Professor, Mechanical Engineering

Department, Jadavpur University

Kolkata-700032

Countersigned by –

…….

DIRECTOR

Prof. Dipten Mishra

School of Laser Science And Engineering

Jadavpur University, Kol-700032

.....

DEAN

Faculty of Interdisciplinary Studies, Law and Management

Jadavpur university, Kol-700032

JADAVPUR UNIVERSITY

FACULTY COUNCIL OF INTERDISCIPLINARY STUDIES, LAW AND MANAGEMENT

Certificate of Approval

*The foregoing thesis, entitled as "**Laser Welding of Dissimilar Materials: Mathematical & Numerical Modelling**" is hereby approved by the committee of final examination for evaluation of thesis as a creditable study of an engineering subject carried out and presented by Mr. Saurav Kumar Ghosh (Registration No – 160420 of 2021- 2022) in a manner satisfactory to warrant its acceptance as a perquisite to the degree of Master of Technology in Laser Science And Technology. It is understood that by this approval, the undersigned do not necessarily endorse or approve any statement made, opinion expressed or conclusion drawn therein, but approve the thesis only for the purpose for which it is submitted.*

Committee of final examination for evaluation of thesis –

……..……..…….. ..…….....……..

……..……..…….. ..…….....……..

Dedicated to My Parents

ACKNOWLEDEGMENT

I owe a deep sense of gratitude to my respected thesis advisor ***Dr. Nilkanta Barman*** *for his esteemed guidance and encouragement throughout this work. Without his generous support and motivation this would not have been completed.It was a great privilege and experience to work under them.*

I am indebted to ***Prof. Dipten Mishra****, Director of School of Laser Science and Engineering, Jadavpur University for providing the facilities during the course of investigation.*

I am also grateful to all the faculty members of School of Laser Science and Engineering, Jadavpur University and Research Scholars of School of Laser Science and Engineering, Jadavpur University for their moral support, help and cooperation. In this regard, I also thank all of the School of Laser Science and Engineering for their constant support.

Thanks to all my friends who helped me with their valuable suggestions. I want to convey my heartiest gratitude to all my batch mates and junior friends for kind cooperation and making my two years at Jadavpur University memorable.

Last but not the least, I thank my mother and father for being a source of continuous moral courage and inspiration. Above all, I thank the Almighty God for showering His blessings during the days of this work.

Date:

_____

Saurav Kumar Ghosh

School of Laser Science & Engineering

Jadavpur university, Kolkata-700032

List of Figures

List of Tables

Abstract

This work includes numerical simulation of a laser welding process in order to understand the transport phenomena during joining of two dissimilar materials, i.e., Ti-6Al-4V titanium alloy and AISI 316L stainless steel in the present thesis. Accordingly, a numerical code is developed on the FORTRAN platform. The numerical code is developed based on the finite volume method considering the SIMPLER algorithm includes using of the power law scheme and the staggered grids for velocity vector, and the subsequent solution of finally obtained discretized simultaneous equations is performed on the TDMA algorithm. The setting of boundary conditions plays an important role in the present problem as the whole generated heat of the laser is transferred to the ambient through convection and radiation only that is represented here by an equivalent heat transfer coefficient. Hence, an emphasis is drawn on inclusion of the boundary conditions within the code. Accordingly, a simple slab of Ti-6Al-4V titanium alloy with thickness of 80mm is considered for validation of the code where the initial temperature of the slab and heat transfer coefficient related to the ambient fluid are considered as 1632°C and 20 W/m2 -°C. The variation of temperature with time at centre of the slab is compared with the available as the standard solution in the book of heat transfer by Ozisik (1984). A very good agreement is found between the numerical and analytical solutions. The developed code is then tested for necessary grid independent study.

Chapter-I

Introduction

1.1 Background

In this decade, the use of high power density welding technologies such as laser welding has been increasingly sharply and utilizing it widely in the construction and industrial engineering. The laser welding process offers a great potential in designing and fabricating of new products. Compared to the other welding processes such as arc welding, solid state welding, induction welding, friction stir welding etc., a small heat affected zone (HAZ) is developed into the work piece in case of laser welding, and resulting low panel distortion [1]. But, in case of laser welding, the transport phenomena are complex in nature include phase transition such as melting and evaporation, laser light absorption and reflection, and moreover, the material properties are temperature dependent. All of such phenomena occur in a very short time [2]. As found in literature, the tradition trial and error based experimental approaches have encountered many difficulties in optimizing the laser welding process. Thus, in order to extend of the laser welding in the industrial applications and make such process more reliable, there is a necessity to understand the process of laser welding in details and develop necessary concepts for its applications, which is the primary of objective of the present thesis.

Further, joining of the reflective and dissimilar metals is difficult and even impossible using other kind of welding methods, whereas the laser welding is very much useful in such cases. This laser welding is useful in joining a variety of metals include stainless steel, nickel, titanium, inconel, and molybdenum etc. and notably, welding of the reflective and dissimilar materials such as copper and aluminum, is possible using laser [3]. The laser is also used in welding of the microfluidics chips and surgical equipment. In addition, the laser welding is a noncontact process and possible to customize the system parameters. Based on the requirement, a user may easily control size of the laser beam, and hence, size of the heat affected zone (HAZ). In laser welding, heat transmits in a small and controlled area whereas other welding processes such as MIG welding have wider heat input area, which causes more residual stress on its products [4]. It is further known that a controlled welding possibly keeps the metallurgical structure intact. Thus, a laser welding results a high quality weld which requires less finishing and heat treating. In laser welding, control of heat affected zone is possible leads to weld an exterior of any device without affecting the thermal-sensitive other internal components. In brief, the use of laser welding provides more advantages than other welding processes. Accordingly, the research and development of the laser processing is in progress, now-a-days [5-10].

Alongside, the recent requirement of the ability to manufacture a product by different metals and alloys is greatly increasing, and leads flexibility in design and production where optimization of the properties such as wear and corrosion resistance is possible, and beneficial in terms of producing economic products. Now, joining of the dissimilar metals is a challenge, now-a-days, with respect to retain good physical and chemical properties in the welds. The laser welding, which is a high power density with low energy-input process, provides a necessary solution to a number of common problems encountered in the conventional joining processes,

and results accurate positioning of the weld bead, rapid heating as well as cooling, low distortion, process flexibility, and hence, better product design for application purpose. But, it is well known that understanding of the transport phenomena in laser welding is complex in nature as this welding process include phase transition such as melting and evaporation, absorption and reflection of the laser beam, and moreover, all properties of the materials are temperature dependent and all of such phenomena occur in a very short time. Hence, there is a need to understand the process of laser welding in details and develop the necessary concepts for its practical applications. On the other hand, all experimental approaches have encountered many difficulties in optimizing laser welding process. Accordingly, this work considers a numerical study in respect of understanding the transport phenomena during a laser welding process. In order to understand related basics of the laser welding, a rigorous review of literature is carried out and presented in the section 1.2.

1.2 Literature Review

The transport phenomena in a laser welding are complex in nature. Accordingly, its preliminary understanding includes a thorough review of literature. Based on the availability, the majority of the reported literature involves experimental as well as numerical investigations of similar and dissimilar materials. The present review of the literature is presented accordingly: the sub-sections 1.2.1 and 1.2.2 present mainly the experimental based literature where the welding of similar and dissimilar materials, respectively, is considered; the sub-sections 1.2.3 and 1.2.4 present mainly the numerical analysis based literature where welding of similar and dissimilar materials, respectively, is considered.

1.2.1 Review related to Experimental Analysis for Similar Materials

Tsoukantas and Chryssolouris [11] presented an experimental analysis of a remote welding process on thin lap joint of AISI 304 sheets. A comparison is made with existing experimental data and found a good agreement.

Tilli *et al*. [12] presented an experimental analysis of temperature distribution and melt flow in fiber laser welding of inconel 625. In this study, the effects of welding speed and laser power in continuous wave laser welding process of Inconel 625 sheets are investigated by experimental method as well as by the finite volume method. As the welding speed increases, the constant temperature lines on the surface of work part becomes ellipsoid which led to a decrease in the HAZ. By increasing temperature from 700°C to a range of 1200°C and 1800°C, a change in the microstructure change is observed from base metal to the HAZ region, results formation of austenitic coarse-grained structure relative to the base metal austenitic structure.

Chandelkar and Pradhan [13] presented experimental analysis of the laser welding of SS317L alloy using 400W Nd-Yag laser beam. They found related dominating factors are temperature, welding current and pulse width those affect tensile strength of the welds.

Sinha *et al.* [14] presented experimental analysis of the laser welding of galvanized steel in a lap joint configuration in order to investigate the potential of the variation of weld seam as joining quality estimator. In this paper, the relationship between variation of weld seam and tensile shear strength of the laser welding of galvanized steel is investigated.

Chuan *et al.* [15] presented experimental analysis of residual stresses in full penetration laser beam welding of Ti6Al4V alloy. A uniform conical heat source modeled with parameters out of the actual weld seam dimensions is developed to simulate the welding temperature fields with different welding heat inputs. The results presented that cross section profiles of the weld

seam simulated as the conical heat source agree well with the experimental results, the zone of residual stresses distribution in laser full penetration welding of Ti6Al4V alloy is very narrow, and gradient of the longitudinal residual stress is very steep.

Mehrpouya [16] presented experimental analysis of laser welding of NiTi shape memory sheets and reports the effect of laser parameters on microstructural, functionality, and mechanical properties of the welded joints. Also, this study is employed a numerical model to estimate the optimum laser parameters, including the laser power and scan speed those produce the HAZ and FZ. The simulation results, including variation of transient temperature, welding penetration, and dimensions of HAZ and FZ, presented a good accuracy compared with that of experimental results.

Franz *et al.* [17] presented experimental analysis of zero gap laser welding of zinc coated steels in a lap joint configuration. In the paper, the authors found welds with a smaller spot diameter leads to a sufficient increase of the joint quality by using the zero gap overlap configuration.

Liu *et al.* [18] presented experimental verification of residual stress in autogenous laser welding of high strength steel. Results showed that the transverse and longitudinal residual stresses prevailed in the autogenous laser welding process, and the thermal stress concentration occurs in the molten pool and its adjacent regions.

1.2.2 Review related to Experimental Analysis for Dissimilar Materials

Zhang *et al.* [19] presented an experimental analysis of a fiber laser butt welding of AISI 304 and Q235 low carbon steel. The effects of laser power and laser beam offset to the sides of center of welding gap on the welded joint shape and strength are experimentally investigated, and the optimum laser power and laser beam offset are determined based on tensile strength

and hardness tests of the weldment. The different thermal conductivity and melting temperatures of the two dissimilar metals result in different shapes of the welded joint. A numerical simulation with a combined asymmetric heat source is implemented, and the results agreed well with the experimental results. The study investigates mechanisms for forming different weld joint shapes in AISI304L and Q235 steels. They presented different shapes of weld joints of different thermal conductivity and melting temperatures dissimilar metals.

Shaibu *et al.* [20] presented an experimental analysis of CO_2 laser welding applied to copper and 304 stainless steel. The study involves a numerical study also where a volumetric Gaussian heat source is applied symmetrically on the both metal domain, and an asymmetric molten pool shape is found. It is observed that the computational model has good concurrence with the experimental results.

Lambaise and Genna [21] presented experimental analysis of the laser assisted joining of polytheretherketone (PEEK) and AA5083 aluminum alloy. Maximum shear strength of the joint is found to a value of about 30MPa when used laser power is 200W with an energy of 2000J. Under the conditions, the joint efficiency reaches to 53%. This value is much higher than that achieved with any high-performance adhesive. Increasing of welding energy enables to enlarge joint area, consequently this increases maximum shear force with formation of bubbles. These bubbles produce an adverse effect that dramatically limits the strength of the joints.

Casalino and Mortello [22] presented experimental analysis of a fiber laser offset welding of AA5754 and Ti6Al4V alloys of 2mm thickness, joined in butt configuration. A good bead appearance with good mechanical properties is found. This increases the productivity and versatility of the welding process. The seam quality and brittle interface of the joints depend on both the laser offset and linear energy.

Borrisutthekul *et al.* [23] presented experimental analysis of a laser welding between magnesium alloy (AZ31B) and aluminum alloy (A5052-O). Further, a possible method to suppress the inter metallic compound (IMC) formation is investigated based on the FEM analysis and found a shallow penetration depth of molten metal into lower plate in case of the edge-line welding lap joint, which reduces reaction between two metals and also reduces formation of inter metallic compound. From the experimental results, a shallow penetration depth into lower plate is also found, subsequently concluded possible obtaining of a thin inter metallic layer and a higher joining strength using the edge-line welding lap joint.

Zeng *et al.* [24] presented experimental as well as numerical analysis on a three-dimensional finite element analyses to produce residual stresses on AZ31B magnesium alloy and 304L steel butt joint by the hybrid laser TIG and TIG welding illustrating variation of the residual stress distribution and deformation on the plates. It is seen that the hybrid welded joint is advantageous compared to the TIG welded joints in respect of less residual stress and welding deformation.

Zhao *et al.* [25] presented experimental investigation of a laser overlap welding of Ti6Al4V and 42CrMo. The laser overlap welding technique is used for joining titanium alloy and alloy steel, and further understanding of the welding process is achieved by FEM model and compared with experimental investigations. Thickness of the inter metallic reaction layer containing Ti/Fe inter metallic compounds decreases by reducing of the heat input. The temperature history at the measuring points obtained by the FEM model considering contact resistance and forced convection effect. A good qualitative agreement of the numerical prediction with the experimental is observed.

Yang *et al.* [26] presented experimental analysis on influence of the laser power on microstructure and properties of laser welding-brazing of 5052 Al alloys to Al-Si coated 22MnB5 steel. It is found that with increase in laser power, the tensile strength raises first and then decreases.

Zhou *et al*. [27] presented dissimilar laser lap welding of Mg and Al alloys using a CoCrFeNi medium entropy alloy interlayer. The material microstructure property relations are established in this work.

Borrisutthekul *et al.* [28] presented dissimilar material laser welding between magnesium alloy (AZ31B) and aluminum alloy (A5052-O). The joining technology of the lightweight dissimilar metals between magnesium and aluminum alloy is adopted here, which is essential for realizing the hybrid structure cars and others engineering applications.

Saleh *et al.* [29] presented experimental analysis of the laser welding on dissimilar materials with influence of adding interlayer. In this study, the impact of incorporating a nickel (Ni) foil as an intermediate layer on the lap joints of dissimilar materials (SS304 and A16061) is investigated using continuous laser welding (CLW) technique.

Kuryntsev [30] presented a review of the laser welding of dissimilar materials (Al/Fe, Al/Ti, Al/Cu). The paper analyzes the influence of the basic techniques, method, and the uses of laser welding properties.

1.2.3 Review related to Numerical Simulation for Similar Materials

Ghosh *et al*. [31] presented a numerical simulation of a laser welding of 2205 duplex stainless steel. In this work, the laser welding process is investigated considering phase change during butt joint welding of 2205 duplex stainless steel plates through the process modelling using the finite element method (FEM) and statistical techniques. They presented an investigation on effect of

the process parameters such as laser power, scanning speed and beam diameter on the evolution of thermal field and formation of the weld bead geometry. Simulation results show that maximum temperature at weld zone, bead width and depth of penetration increases with the laser power, and decreases with scanning speed. It is also seen that with increase of beam diameter, maximum temperature at weld zone and depth of penetration decreases, while bead width increases.

Azizpour *et al.* [32] presented a numerical simulation of the laser beam welding of Ti6Al4V sheet. This paper reported a 3D finite element analysis simulation for laser welding of 1.7 mm Ti6Al4V sheets in the form of a butt joint in order to predict temperature distribution, also hardness, and weld geometry. Also the butt-joint welds are made experimentally using the CO_2 laser with maximum power of 2.2kW in the continuous wave mode. The experimental work is carried out to verify the weld geometry with the specific weld parameters including power, speed, and focal position. The effect of the focal position on the weld bead geometry is also investigated. As found, the variation of the focal position does not significantly alter the penetration depth and weld bead geometry. The high velocity of laser beam causes weld bead smaller. The hardness at center of the weld pool is maximum, and higher laser speed causes more difference in hardness between the weld pool and base metal.

Spina *et al.* [33] presented thermo-mechanical modeling of AA5083 sheets. A 3D finite element (FE) model is developed to simulate the laser welding process of AA5083 thin sheets, and predicted their final distortion. After comparison of results out of the FE model and the experiments for a specific welding speed, the FE model is used to produce the thermal loads induced by the laser source at different welding speeds. A very good agreement is found with the experimental results for all cases.

Mehrpouya *et al.* [34] presented a numerical study for prediction of optimum operational parameters in laser welding of NiTi alloy by the finite element simulation and artificial neutral network. Their necessary microstructural study illustrates that the laser welding process effects grains size of the HAZ regions. In fact, the HAZ area shows a coarser grain compared with the HAZ region due to the effect of the temperature gradient and solidification rate. It is observed that the HAZ area close to the base metal contains fine equiaxed structure. The dimension of the fusion zone (FZ) and HAZ slightly reduces when both laser power and scan speed combinedly increases. They found that the maximum temperature occurs when the laser welding and scan speed are 500W and 3 mm/s, respectively.

Tilli *et al.* [35] presented an experimental analysis on temperature distribution and melt flow in a fiber laser welding of inconel 625. In this study, the effect of the welding speed and laser power during continuous wave laser welding process of the Inconel 625 sheets is investigated by finite volume and experimental methods. As the welding speed increases, the constant temperature lines on surface of the work pieces becomes ellipsoid which leads to a decrease in the HAZ.

Chandelkar and Pradhan [36] presented an experimental analysis of a laser welding of SS317L alloy using 400W Nd-Yag laser beam. They found some dominating factors that affect the temperature, are welding current and pulse width, and he dominating factors that affect the tensile strength are frequency and welding current.

Zhang *et al.* [37] presented a numerical simulation of full penetration laser welding of thick steel plate with high power high brightness laser. In full penetration welding, the lower surface of molten pool is more unstable than the upper surface. The transient evolution of the

molten pool and keyhole in quasi-steady stage of the laser in the full penetration welding, a periodic feature is observed.

Chuan *et al.* [38] presented numerical analysis of residual stresses in full penetration laser beam welding of Ti6Al4V alloy. A uniform conical heat source model with parameters considered from the actual weld seam dimensions is developed to simulate the fields of welding temperature with different welding heat inputs. The results show that the cross section profiles of the weld seam simulated with the conical heat source based on the configuration of weld seam agree well with the experimental results, the zone of residual stresses distribution in laser full penetration welding of Ti6Al4V alloy is very narrow and the gradient of longitudinal residual stress is very steep.

Mehrpouya [39] presented experimental analysis of the laser welding of NiTi shape memory sheets and reports the effect of laser parameters on microstructural, functionality, and mechanical properties of the welded joints. Also, this study is employed a numerical model to estimate the optimum laser parameters, including laser power and scan speed, which can produce the HAZ and FZ and therefore result in better weld. The simulation results, including the transient temperature, welding penetration and the dimension of HAZ and FZ, show a good accuracy compared to the experimental results.

Liu *et al.* [40] presented numerical modelling of residual stress in autogenous laser welding off high strength steel. Results showed that the transverse and longitudinal residual stresses prevailed in autogenous laser welding process, and the thermal stress concentration occoured in the molten pool and its adjacent regions.

Rong *et al.* [41] presented numerical simulation of angular distortion and residual stress in hybrid laser magnetic welding of 316L steel with but joint. The laser magnetic welding is

useful to homogenize the weld of bead geometry, microstructure, angular distortion, residual stress and plastic strain.

Panda *et al.* [42] presented numerical simulations and experimental results of tensile test behaviour of laser but welded DP 980 steels. It is observed from tensile test experiments and numerical simulations that both a decrease in strength and an increase in width of the softened HAZ were responsible for a decrease in the overall strength and ductility of the welded blanks.

1.2.4 Review related to Numerical Simulation for Dissimilar Materials

Behulova *et al.* [43] offered a numerical simulation of temperature field during a laser welding-brazing of Al/Ti plates. This is a successful effort to join aluminum alloy to titanium alloy, associated with necessary demand of minimizing the thickness by selecting appropriate welding parameters and applying suitable filler materials. The numerical simulation of the laser welding-brazing process is found sufficiently accurate and useful to study effects of the welding parameters on the temperature field and ultimate tensile strength of the welded and brazed joints. The laser power significantly impacts on the temperature field during the laser welding-brazing process, while the effect to the laser beam offset and welding speed is less. The ultimate tensile strength of the welded-brazed joints is primarily affected by the amount of melted Ti. The thickness and morphology forms during rapid solidification of the melt are directly related to the amount of melted titanium. An increase in the laser beam offset towards the Al side leads to a decrease in the amount of melted Ti, while the melted zone on the Al side increases, and, thus, resulting an increase in the ultimate tensile strength of the welded-brazed joint.

Danielewski *et al.* [44] presented a numerical simulation of a laser welding for dissimilar low carbon and austenitic steel joint. Numerical analysis involves thermo-mechanical method and phase transformation for estimating the weld dimension and joint properties. Simulation of low carbon and stainless steel joints using the Simu-fact Welding software are presented. Model of heat source within the geometry and parameters is programmed. Laser beam welding simulation is performed for estimating parameters for the complete joints penetration. Welding boundary condition and heat source geometry, welding parameters and welding speed rate are estimated. Materials used in the simulation process and experimental welding are low carbon S235JR and stainless 316L steels in sheet form. Joint properties such as fusion zone and heat affected zone dimension and stress-strain distribution are presented. The obtained hardness exceeds 350HV10, and for the industrial applications, additional heat treatment of the welds is required.

Wang *et al.* [45] presented a numerical simulation analysis of a laser welding of a 5182 aluminum alloy and 30% glass fiber reinforced PA66 material. The influence of the laser welding power and velocity on the welding strength of PA66 aluminum alloy after surface texture treatment is studied. The tensile shear test results show that the welding strength of aluminum alloy and PA66, increases firstly and then decreases with the increase of laser power and velocity. The welding strength is the highest when the laser power is 1200W and the welding velocity is 2.5 mm/s, and the maximum welding strength is 1341N. When laser input energy increases, melt zone of the plastic becomes larger. Temperature of the metal and plastic contact interface exceeds thermal decomposition temperature of the plastic when the laser input energy is high. The thermal decomposition zone appears inside of the plastic melting zone.

Mosavi *et al.* [46] presented a numerical simulation analysis of a fiber laser welding of

AISI 304 and AISI 420. The effect of the fiber laser welding parameters on temperature around the welded zone is studied using the CCD and response surface method (RSM). The relation in variation of temperature field near to the molten pool is clearly show indirect behavior of laser beam penetration and absorption by the materials produce melt pool.

Zhang *et al.* [47] presented numerical investigation of fiber laser butt welding of AISI 304 and Q235 low carbon steel. The effects of the laser power and laser beam offset to the sides of the center of the welding gap on the welded joint shape and strength are experimentally investigated, and the optimum laser power and laser beam offset are determined via tensile strengthand hardness tests of the weldment. The different thermal conductivity and melting temperatures of the two dissimilar metals result a differential shape in the welded joint. The numerical simulation with a combined asymmetric heat source is implemented in this study, results agreed well with the experimental results. Then the model is applied to investigate mechanisms in forming of weld shape in different weld joints of AISI304L and Q235 steels. The differential shape in the weld joints caused due to different thermal conductivity and melting temperature of the dissimilar metals.

Shaibu *et al.* [48] presented a numerical simulation analysis where CO_2 laser welding is applied to the copper and 304 stainless steel. For making the dissimilar couple, a volumetric Gaussian heat source is applied symmetrically on the both metal domain and it is found an asymmetric molten pool shape. It is observed that the computational model provides a good concurrence with the experimental results for the same set of parameters.

Zhao *et al.* [49] presented a numerical investigation of a laser overlap welding of Ti6Al4V and 42CrMo. Welding depth is defined as a parameter to reflect the temperature

field, which increases linearly with the laser power at a constant scanning velocity. The molten pool is formed just at interface by adjusting process parameters.

Faraji *et al.* [50] presented a numerical modeling of fluid flow, heat and mass transfer for a laser welding of Ti6Al4V and inconel 718. The laser source is simulated by a volumetric heat distribution, which considers effects of the keyhole and heat transfer on work piece. Both the weld pool width and depth increase with the laser power, but the effect on the depth is more significant than on the width. The dissimilar welding simulation shows a higher temperature gradient in the nickel side due to its higher thermal conductivity. The temperature gradient plays an important role in developing residual stress during cooling stage.

1.3 Objective of the Present Thesis

Now-a-days, the laser welding process has a great potential and a wide usefulness in designing and fabricating of new products. It is found comparing with the other welding processes such as arc welding, solid state welding, induction welding, friction stir welding etc. that a small heat affected zone is developed into work pieces in case of laser welding. A user may easily control size of the laser beam, and hence, respective size of the heat affected zone. It is further known that a controllable welding possibly keeps metallurgical structure of the work pieces intact. Thus, a laser welding results a high quality weld that requires less finishing and heat treatment. It provides weld joints with low distortion and good mechanical and metallurgical properties.

It is also known that joining of reflective and dissimilar metals is much difficult and even impossible by the conventional welding methods, whereas the laser welding is very much useful in such cases. The laser welding allows joining a variety of metals include stainless steel, nickel, titanium, inconel, and molybdenum etc. Moreover, this welding is usable for very thin sheets too.

Now, this laser welding involves melting and solidification of the joining materials. The corresponding transport phenomena are complex in nature include phase transformation during melting due to high laser source and during solidification too, and all material properties are temperature dependent. Moreover, all of such phenomena occur in a very short time. In addition, out of the literature review, it is found that weld properties depend on various weld parameters such as laser power, scanning speed, focal position etc., accordingly the weld bead geometry is formed, leads to the desire properties of the welds. Thus, in order to extend of the laser welding in industrial applications and make such process is more reliable, there is a need to understand the process of laser welding in details and develop necessary concepts for its applications, which is the primary of objective of the present thesis.

Further, based on the literature review, it is found that the welding of dissimilar materials is very much difficult because of their different thermo-physical properties and melting points, which emphasizes for a detailed study of the transport phenomena during welding of dissimilar materials. This work, thus, is a consideration of a study of the laser welding of dissimilar metals. As found in the literature, the tradition trial and error based experimental approaches have encountered many difficulties in understanding the basics of laser welding process. Accordingly, this work considers a numerical study based on the finite volume method (FVM), involves:

(i) Suitable mathematical modeling of the laser source

(ii) Mathematical modelling of melting and solidification processes of concerned metals during laser welding

(iii) Numerical modelling of related governing equations/mathematical models

(iv) Development of a programing code on the FORTRAN platform

(v) Prediction of the results: temperature distribution, area of HAZ, penetration depth, weld bead geometry under different process parameters.

1.4 Layout of the Thesis

Chapter-II: Description of the Physical Problem, its Mathematical and Numerical Modelling

Chapter-III: Results and Discussion

Chapter-IV: Conclusion and Future Works

References

[1] W. Liu, J. Ma, F. Kong, S. Liu, and R. Kovacevic, Numerical modeling and experimental verification of residual stress in autogenous laser welding of high strength steel, *Laser Manuf. Mater. Process*, Vol. 2 (2015), pp. 24-42.

[2] W. Ke, Z. Zeng, J. P. Oliveira, B. Peng, J. Shen, C. Tan, X. Song, and W. Yan, Heat transfer and melt flow of keyhole, transition and conduction modes in laser beam oscillating welding, *International Journal of Heat and Mass Transfer*, Vol. 203 (2023), 123821

[3] W. Liu, J. Ma, G. Yang, and R. Kovacevic, Hybrid laser-arc welding of advanced high-strength steel, *J. Mater. Process. Technol.*, Vol. 214(12) (2014), pp. 2823–2833

[4] D. Zaza, M. Ciavarella, and G. Zurlo, Strain incompatibility as a source of residual stress in welding and additive manufacturing, *European Journal of Mechanics - A/Solids*, Vol. 85 (2021), 104147

[5] A. Stepanov, E. Saukkonen, and H. Piili, Possibilities of laser processing of paper materials, *Physics Procedia*, Vol. 78(2015), pp. 138-146.

[6] Z. Wang, Y. Ma, B. Yuan, C. Wu, C. Li, and S. Sun, Development of Laser Processing Carbon-Fiber-Reinforced Plastic, *Sensors*, Vol. 23 (7) (2023), 3659

[7] J. C. Ion, Laser Processing of Engineering Materials, Butterworth-Heinemann, 1st Ed., 2005

[8] Malinauskas, Mangirdas, Zukauskas, Albertas, Hasegawa, Satoshi, Hayasaki, and Yoshio, Ultrafast laser processing of materials: from science to industry, *Light: Science & Application*, Vol. 5(8) (2016), 133

[9] Katayama, Seji, Nagayama, Hiroyuki, Mizutani, Masami, Kawahito, and Yousuke, Fibre laser welding of aluminium alloy, *Journal Metal Welding and Construction*, Vol. 46 (2008), pp. 470-479.

[10] Kawahito, Yousuke, Miutani, Masami, Katayama, and Seji, Elucidation of high-power fibre laser welding phenomena of stainless steel and effect of factors on weld geometry, *J. Phys. D. Apply physics*, Vol. 40(2007), pp. 5854-5859

[11] G. Tsoukantas and G. Chryssolouris, Theoretical and experimental analysis of the remote welding process on thin, lap joined AISI 304 sheets, *Int. J. Adv. Manuf. Technology*, Vol.35 (2008), pp. 880-894

[12] I. Tilli, D. Baleanu, S. Mohammad Sajadi, F. Ghaemi, And M. A. Fagiry, Numerical and Experimental analysis of temperature distribution and melt flow in fiber laser welding of Inconel 625, *The International Journal of Advance Manufacturing Technology*, Vol. 121 (2022), pp. 765-784

[13] V. Chandelkar, and S. K. Pradhan, Numerical simulation of temperature distribution and experimentation in laser beam welding of SS317L alloy, *Materials Today: Proceedings*, Vol. 27(2020), pp. 2758-2762

[14] A. K. Sinha, D. Y. Kim, and D. Ceglarek, Correlation analysis of the variation of weld seam and tensile strength in laser welding of galvanized steel, *Optics and Lasers in Engineering*, Vol. 51(2013), pp. 1143-1152

[15] L. Chuan, Z. Jianxun, and N. Jing, Numerical and experimental analysis of residual stresses in full penetration laser beam welding of Ti6Al4V alloy, Rare Metal Materials and Engineering, Vol.38(8) (2009), pp. 1317-1320

[16] M. Mehrpouya, Laser welding of NiTi shape memory sheets: Experimental analysis and numerical modeling, *A PhD Thesis, Department of Mechanical and Aerospace Engineering, Sapienza University of Rome*, 2017, DOI: 10.13140/RG.2.2.27418.49605

[17] A. Franz, D. Paethe, and K. Dilger, Experimental analysis of zero gap laser welding of zinc coated steels in a lap joint configuration, *Materials Design and Applications*, Vol. 234(5) (2020), pp. 658-664.

[18] W. Liu, J. Mia, F. Kong, S. Liu, and R. Kovacevic, Numerical modeling and experimental verification of residual stress in autogenous laser welding of high strength steel, Laser Manuf. Mater. Process, Vol. 2(2015), pp.24-42

[19] Y. Zhang, X. Gau, D. You, X. Jiang and W. Ge, Investigation of laser butt welding of AISI 304L & Q235 steels based on numerical & experimental analysis, *Metals*, Vol.12 (2022), pp. 803

[20] V. B. Shaibu, S. K. Sahoo, and A. Kumar, Computational modeling of dissimilar metal CO_2 laser welding applied to copper and 304 stainless steel, *Procedia Engineering*, Vol.127 (2015), pp. 208-214

[21] F. Lambiase, and S. Genna, Experimental analysis of laser assisted joining of Al-Mg aluminum alloy with Polyetheretherketone (PEEK), International Journal of Adhesion and Adhesives, Vol. 84 (2018), pp.265-274

[22] G. Casalino and M. Mortello, Modeling and experimental analysis of fiber laser offset welding of Al- Ti butt joints, *The International Journal of Advanced Manufacturing Technology*, Vol. 83(1) (2016), pp.89–98

[23] R. Borrisutthekul, Y. Miyashita, and Y. Mutoh, Dissimilar material laser welding between magnesium alloy Az31B and aluminum alloy A5052-O, *Science and Technology of Advanced Materials*, Vol. 6 (2005), pp. 199-204

[24] Z. Zeng, X. Li, Y. Miao, G. Wu, and Z. Zhao, Numerical and experimental analysis of residual stress on magnesium alloy and steel butt joint by hybrid laser TIG welding, *Computational Materials Science*, Vol.50 (2011), pp.1763-1769

[25] S. Zhao, G. Yu, X. He, Y. Zhang, and W. Ning, Numerical simulation and experimental investigation of laser overlap welding of Ti6Al4V and 42CrMo, *Journal of Materials Technology*, Vol. 211(2011), pp. 530-537

[26] J. Yang, M. Xiao, L. Wu, Z. Li, H. Liu, Y. Zhao, W. Guo, and C. Tan, The influence of laser power on microstructure and properties of laser welding brazing of Al alloy to Al- Si coated 22MnB5 steel, *Optics and Laser Technology*, Vol. 162(2023),109318

[27] J. Zhou, C. Chen, Z. Zhou, H. Long, J. Jia, L. He, and Y. long, Dissimilar laser lap welding of Mg and Al alloys using a CoCrFeNi medium entropy alloy interlayer, Optics and Laser Technology, Vol. 157(2023), 108639

[28] Y. Itoh and K. Toshiba, Joint structure of dissimilar metallic materials, Patent Publication Number, EP0923145A2,1999

[29] T. A. Mai and A. C. Spowage, Characterization of dissimilar joints in laser welding of steel -copper, copper-steel and copper-aluminium materials, *Science and Engineering*, Vol. 374 (2004), pp. 224-233.

[30] S. J. Lee, M. Takahasi, Y. Kawahito, and S. Katayama, Microstructural evolution and characteristics of weld fusion zone in high speed dissimilar welding of Ti and Al, *Int. J. Precis. Eng. Manuf.*, Vol. 16 (2015), pp.2121-2127.

[31] A. Ghosh, D. Mishra, and S. K. Acharya, Numerical Simulation of the Laser Welding of 2205 Duplex Stainless Steel, *Int. Journal of Laser Science*, Vol.1 (2019), pp. 293-313

[32] M. Azizpour, M. Ghoreishi, A. Khorram, Numerical simulation of laser beam welding of Ti6Al4V sheets, *Journal of Computational and Applied Research in Mechanical Engineering***,** Vol. 4 (2) (2015), pp.145-154

[33] R. Spina, L. Tricarico, G. Basile, and T. Sibillano, Thermo-mechanical modeling of laser welding of a A5083 sheets, *Journal of Materials Processing Technology*, Vol. 191 (2007), pp. 215-219

[34] M. Mehrpouya, A. Gisario, M. Barletta, S. Natali, and F. Veniali, Dissimilar Laser Welding of NiTi Wires, *Lasers in Manufacturing and Materials Processing*, Vol.6 (2019), pp. 99-112

[35] I. Tilli, D. Baleanu, S. Mohammad Sajadi, F. Ghaemi, and M. A. Fagiry, Numerical and Experimental analysis of temperature distribution and melt flow in fiber laser welding of Inconel 625, *The International Journal of Advance Manufacturing Technology*, Vol. 121 (2022), pp. 765-784

[36] V. Chandelkar, and S. K. Pradhan, Numerical simulation of temperature distribution and experimentation in laser beam welding of SS317L alloy, *Materials Today: Proceedings*, Vol. 27(2020), pp. 2758-2762

[37] L. J. Zhang, J. X. Zhang, A. Gumenyuk, M. Rethmeier, and S. J. Na, Numerical simulation of full penetration laser welding of thick steel plate with high power high brightness laser, *Journal of Materials Processing Technology*, Vol. 214 (2014), pp. 1710-1720

[38] L. Chuan, Z. Jianxun, and N. Jing, Numerical and experimental analysis of residual stresses in full penetration laser beam welding of Ti6Al4V alloy, *Rare Metal Materials and Engineering*, Vol. 38 (8) (2009), pp.1317-1320

[39] M. Mehrpouya, Laser welding of NiTi shape memory sheets: Experimental analysis and numerical modeling, *A PhD Thesis, Department of Mechanical and Aerospace Engineering, Sapienza University of Rome*, 2017, DOI: 10.13140/RG.2.2.27418.49605

[40] W. Liu, J. Ma, F. Kong, S. Liu, and R. Kovacevic, Numerical modeling and experimental verification of residual stress in autogenous laser welding of high strength steel, *Laser Manuf. Mater. Process*, Vol. 2 (2015), pp.24-42,

[41] Y. Rong, Y. Huang, J. Xu, H. Zheng, and G. Zhang, Numerical simulation and experimental analysis of angular distortion and stress in hybrid laser magnetic welding, *Journal of Materials Processing Technology*, Vol. 245 (2017), pp. 270-277

[42] S. K. Panda, N. Sreenivasan, M. L. Kuntz, and Y. Zhou, Numerical simulations and experimental results of tensile test behaviour of laser but welded DP 980 steels, *Journal of Engineering Materials and Technology*, Vol. 130 (4) (2008), 041003

[43] M. Behulova, E. Babalova, and M. Sahul, Design of laser welding parameters for joining Ti grade2 and AW 5754 Aluminum alloys using Numerical simulation, *Advances in Materials Science and Engineering*, (2017), Article ID 3451289, https://doi.org/10.1155/2017/3451289

[44] H. Danielewski, A. Skrzypczyk, S. Tofil, G. Witkowski, and S. Rutkowski, Numerical Simulation of Laser Welding Dissimilar Low Carbon and Austenitic Steel Joints, *Open Eng.*, Vol.10 (2020), pp. 491-498

[45] C. Wang, G. Zhang, Q. Zhu, H. Yang, G. Yang, and Y. Liu, Mechanism and Numerical Simulation Analysis of Laser Welding 5182 Aluminum Alloy/PA66 based on Surface Texture Treatment, *Optics & Laser Technology*, Vol. 153 (2022),108273

[46] A. Mosavi, A. Soleimani, A. Karimi, M. Akbari, A. Karimipour, and A. Karimipour, Investigating the effect of process parameters on the mechanical properties and temperature distribution in fiber laser welding of AISI304 and AISI 420 sheet using response surface methodology, *Infrared Physics and Technology*, Vol. 111(2020), pp. 103478

[47] Y. Zhang, X. Gau, D. You, X. Jiang and W. Ge, Investigation of laser butt welding of AISI 304L and Q235 steels based on numerical and experimental analysis, *Metals*, Vol.12 (2022), pp. 803

[48] V. B. Shaibu, S. K. Sahoo, and A. Kumar, Computational modeling of dissimilar metal CO_2 laser welding applied to copper and 304 stainless steel, *Procedia Engineering*, Vol.127 (2015), pp. 208-214

[49] S. Zhao, G. Yu, X. He, Y. Zhang, and W. Ning, Numerical simulation and experimental investigation of laser overlap welding of Ti6Al4V and 42CrMo, *Journal of Materials Technology*, Vol. 211(2011), pp. 530-537

[50] A. H. Faraji, C. Maletta, G. Barbieri, F. Cogini, and L. Bruno, Numerical modeling of fluid flow, heat, and mass transfer for similar and dissimilar laser welding of Ti6Al4V and Inconel 718, *The International Journal of Advanced Manufacturing Technology*, Vol. 114(2021), pp. 899-914

Chapter-II

Laser Welding of Dissimilar Materials: Mathematical and Numerical Modelling

2.1 Introduction

Now-a-days, preparing joints of dissimilar materials throw a challenge to the researchers where laser is being applied widely to satisfy necessary demand of different sectors such as nuclear sectors, space craft industries, petrochemical sectors, automobile sectors, cryogenic industries etc., and the demand of laser welding is increasing gradually. Such welding deals with different thermo-physical properties, and that leads to the challenge in order to form welding joints of suitable dissimilar materials [51-53]. This work, thus, considers joining or welding of dissimilar metals using laser. Now, such a welding process involves melting and solidification of the dissimilar material, i.e., heat and mass transfer under the high density laser source. A better joint demands a clear understanding of the transport phenomena during laser welding. In this regard, a through literature review [1-50, Chapter-I] has been carried out, which concludes that the tradition trial and error based experimental approaches have encountered many difficulties in understanding the basics of the laser welding process. Accordingly, this work considers a numerical study based on the finite volume method (FVM), involves presenting a suitable mathematical model with laser as a volumetric heat source, subsequent consideration of a numerical model, and development of a code on FORTRAN platform. Hence, validation of the developed code, and subsequent prediction of

results: temperature distribution, area of HAZ, penetration depth, weld-bead geometry under different process parameters.

2.2 Description of the Physical Problem

In order to a preliminary understanding of the transport phenomena during laser welding, and simplification in the modelling part, this work considers a numerical analysis of a butt joint of dissimilar materials using laser. This work considers a combination of dissimilar materials (Ti-6Al-4V titanium alloy and AISI 316L stainless steel) that is used widely [54, 55] in chemical industries, nuclear industries, automobile industries and aerospace industries etc. It is found [56] that several intermetallic components such as FeTi, Fe_2Ti, etc. form at high temperature during welding, those are brittle in nature and increase probability of cracking due to thermal stresses. This numerical analysis is carried out, accordingly, to obtain temperature field during laser welding of the butt joint between Ti-6Al-4V titanium alloy and AISI 316L stainless steel.

Fig. 2.1 represents a schematic of the considered butt joint of dissimilar materials. The dimensions of each sample of the joint are considered as 40 mm×80 mm×4 mm, and an argon laser is considered for this welding. The laser beam radius is considered as 125 m. For simplicity in modelling and related code development, a cross-section of the joint (a 2-D domain as shown in the Fig. 2.1a) is considered to present the weld pool developed during welding between the dissimilar materials whereas the effect of scanning velocity is represented in a separate 2-D domain as shown in Fig. 2.1b. The necessary thermos-physical properties are provided in the Table-2.1.

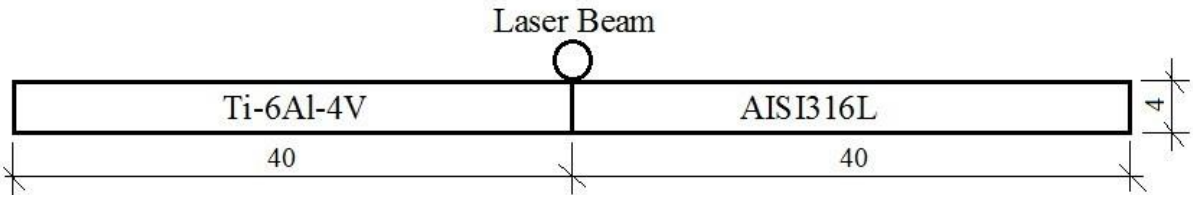

(a)

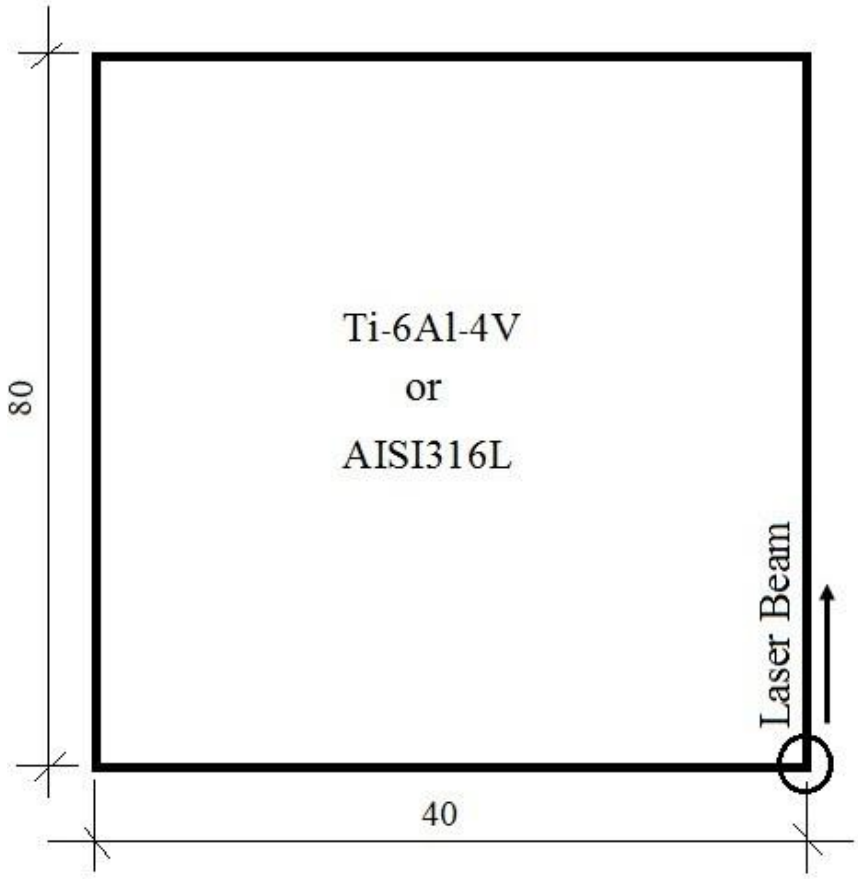

(b)

Figure 2.1: (a) A cross section of the butt joint (a 2-D computational domain on *x*-*z* plane) and (b) one of samples in the butt joint (a 2-D computational domain on *y*-*z* plane)

Table 2.1: The considered thermo-physical properties of the materials for present simulation [57-61]

Description of the properties	***Ti-6Al-4V***	***AISI 316L***
Density (, kg/m^3)	4430	7800
Specific heat (C_P, J/kg. C)	526	585
Thermal conductivity (k, W/m. C)	6.7	15
Solidus temperature (C)	1604	1375
Liquidus temperature (C)	1660	1400
Average meting temperature (C)	1632	1377
Latent heat of fusion (L_a, J/kg)	286000	280000
Thermal expansion coefficient (β_T, 1/ C)	8.6×10^{-6}	1.9×10^{-5}

2.3 Modeling of Laser Beam as a Heat Source

There are mainly three alternatives to model the laser beam as a heat source in welding processes: 2D and 3D Gaussian distribution models, and Goldak's model [62]. In 2D Gaussian distribution model, the energy (W/m^2) distributes according to a Gaussian curve and presents as

$$Q(x,y,t) = Q_0 \exp\left(\frac{-3[(x-x_c)^2+(y-y_c)^2]}{r_0^2}\right) \quad \ldots (2.1)$$

where Q_0 is the introduced area distributed heat flux (as per the Eq. 2.2), and (x, y) and r_0 are the parameters describing position of the heat source [62]. (x_c, y_c) is centre position of the source. An exemplary value of the parameters is shown is the Table 2.2 and corresponding distribution of the energy flux (Q) is shown in the Fig. 2.2.

$$Q_0 = \frac{3\eta P e^3}{\pi(e^3-1)r_0^2} \quad \ldots (2.2)$$

For a welding speed of *v* (m/s), $y_c = vt$ at a time of *t*(s) while the laser beam is moving towards positive *Y*-direction and $x_c = 0$.

Table 2.2: Exemplary values of laser parameters for a 2D model [62]

Description of the parameters	***Value***
Type of laser	Argon
Laser power (*P*, *W*)	750
Beam radius (*m*)	125
Radius of the heat source (r_0, *m*)	471
Process efficiency ( )	0.4
Welding speed (*v*, *m/min*)	2
e	2.7182818
	3.14159265358979

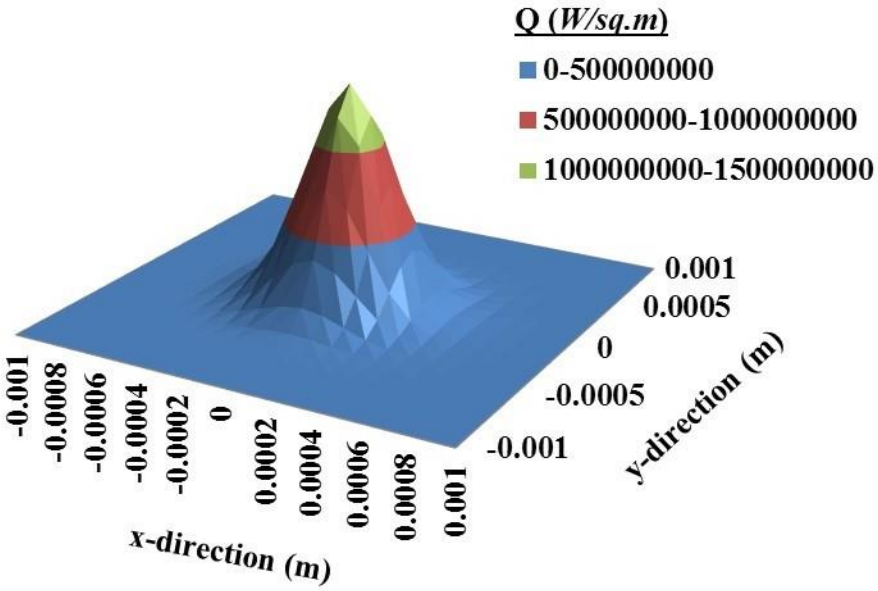

Figure 2.2: Distribution of the energy (Q, W/m^2) for a 2D Gaussian heat source

However, Teixeira *et al.* [63] claimed that the 2D model is not suitable compare to a 3D model for welding of the thick plates as the heat is unable to reach to a deep than that of [27]

the 3D model. It is found in the literature that, in welding processes such as plasma and electron beam welding, and laser welding, assumption of a 3D conical heat source with a Gaussian distribution is more suitable and commonly used in applications. A schematic representation of the 3D conical heat source is shown in Fig. 2.3.

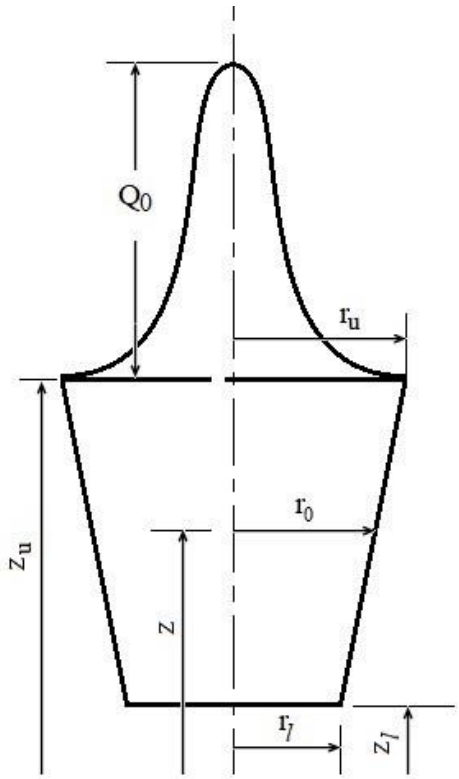

Figure 2.3: Schematic representation of the 3D conical heat source with Gaussian distribution

In case of a 3D conical heat source, distribution of the energy in any x-y plane is similar to the 2D model, i.e., the Gaussian distribution, where the beam radius (r_0) decreases linearly as thickness of the material increases [62], and is represented by Eq. (2.3)

$$r_0 = r_l + (r_u - r_l)\frac{(z - z_l)}{(z_u - z_l)} \quad \ldots (2.3)$$

where r_u and r_l are the upper and lower beam radii, and the upper and lower z-coordinates are z_u and z_l, respectively. An exemplary value of the parameters is shown is the Table 2.3 and corresponding distribution of the volumetric energy (Q) is shown in the Fig. 2.3. The related introduced distributed volumetric heat source (Q_0, W/m^3) of the laser beam is represented as

$$Q_0 = \frac{9\eta P e^3}{\pi(e^3-1)(z_u-z_l)(r_u^2+r_l^2+r_u r_l)} \quad \ldots (2.4)$$

Respective energy (W/m^3) distribution as per the Gaussian curve is presented as

$$Q(x,y,z,t) = Q_0 \exp\left(\frac{-3[(x-x_c)^2+(y-y_c)^2]}{r_0^2}\right) \quad \ldots (2.5)$$

Table 2.3: Exemplary values of laser parameters for a 3D model [62]

Description of the parameters	***Value***
Type of laser	Argon
Laser power (P, W)	750
Beam radius (m)	125
Upper radius of the heat source (r_u, m)	734
Lower radius of the heat source (r_l, m)	356
Process efficiency ( )	0.9
Welding speed (v, m/min)	2
Thickness of the work piece (mm)	2
Upper z-coordinate (z_u, m)	2000
Lower z-coordinate (z_l, m)	0
e	2.7182818
	3.14159265358979

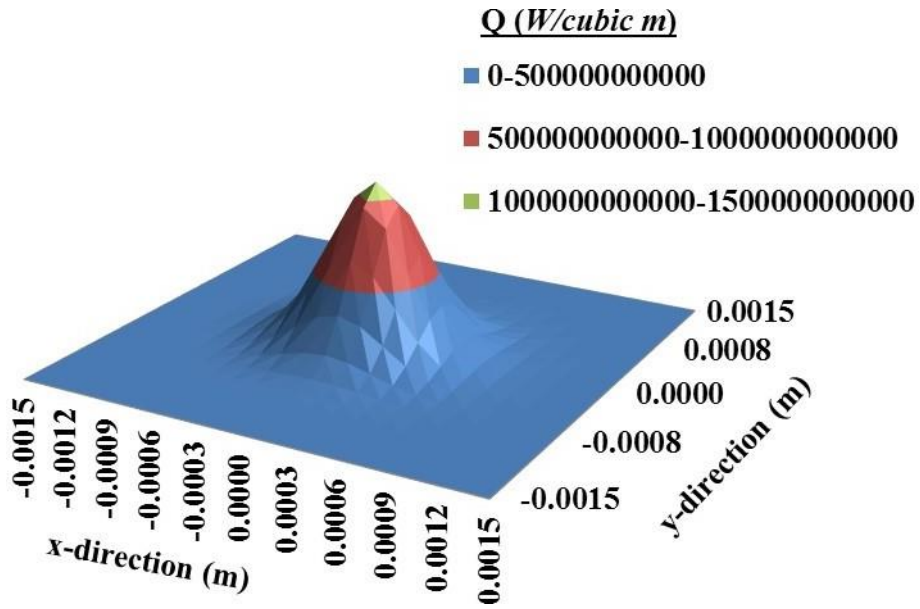

(a)

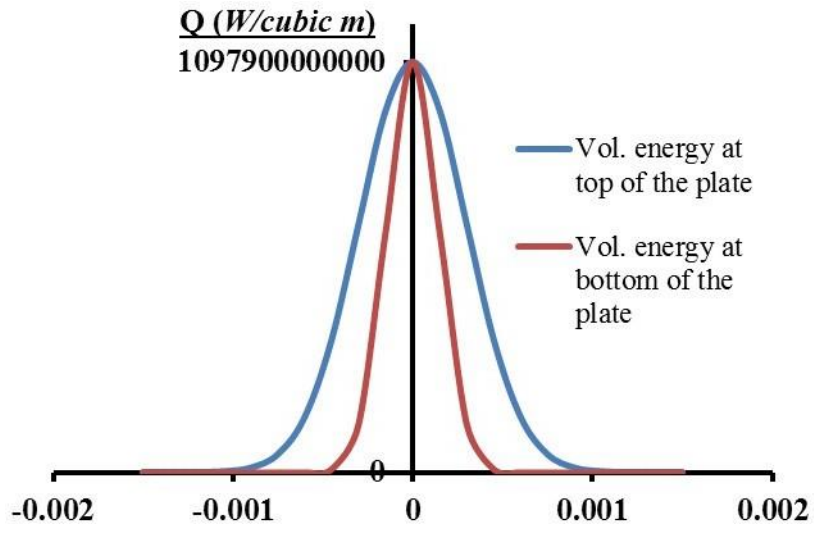

(b)

Figure 2.3: (a) Distribution of the energy (Q, W/m^3) for a 3D conical heat source (at z_u) and (b) comparison of energy distribution (Q, W/m^3) available at z_u and z_l

The Goldak's model [62, 63] is usually presented by two ellipsoids (front and rear) perpendicular to each other as shown in the Fig. 2.4. The equation for the front ellipsoid is presented by Eq. 2.6 and subsequent rear ellipsoid is presented by Eq. 2.7. In these equations (Eq. 2.5 and Eq. 2.6), Q_f and Q_r are front and rear volumetric laser heat flux densities, respectively, and Q is the power introduced by the laser. a, b, c, C_f and C_r are the dimensions of molten pool. The parametersf_f and f_r are the fractions of energy distributed in front and rear parts of the ellipsoid. A usual ratio of f_f and f_r is 60:40 to satisfy a relationship as $f_f + f_r = 2$. Other parameters such as k, l and m are usually determined based on experiments, however, usual accepted value of all is 3.

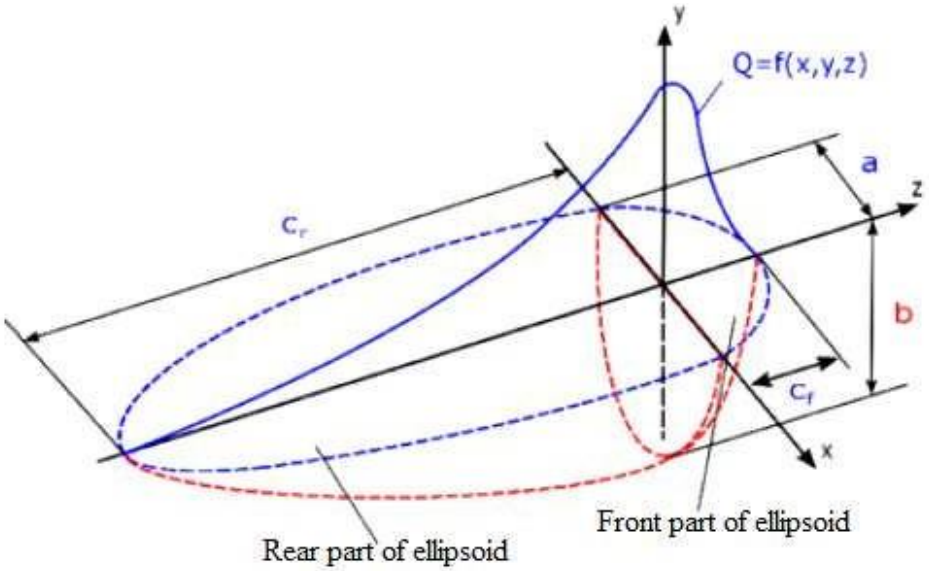

Figure 2.4: Goldak's heat source model [62]

$$Q_f(x,y,z) = \frac{6\sqrt{3}f_f Q}{abC_f\pi\sqrt{\pi}} exp\left(-\frac{kx^2}{a^2} - \frac{ly^2}{b^2} - \frac{mz^2}{c^2}\right) \quad \ldots (2.6)$$

$$Q_r(x,y,z) = \frac{6\sqrt{3}f_r Q}{abC_r\pi\sqrt{\pi}} exp\left(-\frac{kx^2}{a^2} - \frac{ly^2}{b^2} - \frac{mz^2}{c^2}\right) \quad \ldots (2.7)$$

2.4 Mathematical Modelling of the Problem

In the present study, a numerical investigation on a butt joint of two dissimilar materials using a laser beam is considered. Modeling of the laser beam as a heat source is a crucial issue and presented in the section 2.3. This work considers the volumetric 3D conical heat source (in W/m^3) that represents the presence of laser beam during welding of the dissimilar materials [62, 63]. It is represented in the Fig. 2.3 that laser beam is capable of generating high energy density. The dissimilar weld materials consist of different thermos-physical properties definitely behave differently under application of high energy density beam. It includes melting and solidification of the materials, weld pool development, heat evolution and absorption during phase change, development of fluid flow and heat transfer under presence of the heat source and electromagnetic field, macro- and micro-segregations etc. Consideration of all of these phenomena results complexity in the analysis. For simplicity in the analysis, thus, the following major assumptions are considered in the thesis.

(i) All properties of the weld materials are temperature independent.

(ii) Considered the different thermo-physical properties of the weld materials (as per the Table 2.1). Then a continuous domain of interest is assumed by calculating average properties between two nodes. Further, an average melting point is considered to represent each of the weld materials similar to its eutectic material. Accordingly, the macro- and micro-segregations are ignored.

(iii) Mixing of the weld materials is ignored.

(iv) Only the effect of thermal buoyancy is considered for developing fluid flow along with Boussinesq approximation.

(v) Density change during melting and solidification is ignored.

(vi) Molten metals are assumed as the incompressible fluids.

(vii) Representing the laser beam as a volumetric heat source.

Based on the above assumptions, the melting, solidification, fluid flow during the laser welding is represented by the continuity, momentum and energy equations [64-68]. In the model, the enthalpy update scheme [69-70] is used to trace the solid-liquid interface during melting and solidification.

2.4.1 Conservation of Mass

For incompressible fluid, the conservation of mass equation [71-73] for a 2-D computational domain is represented as:

$$\frac{\partial(\rho u)}{\partial x}+\frac{\partial(\rho u)}{\partial x}=0 \qquad \ldots (2.8)$$

In the Eq. 2.8, ρ denotes density (kg/m^3) of the weld materials; u and v denote the velocities (m/s) in x- and y-directions, respectively.

2.4.2 Conservation of Momentum

In the present mathematical model, the following equations [71-73] are considered for the conservation of momentum.

$$\frac{\partial(\rho u)}{\partial t}+u\frac{\partial(\rho u)}{\partial x}+v\frac{\partial(\rho u)}{\partial y}=-\frac{\partial P}{\partial x}+\nabla.(\mu\nabla u)+S_u \qquad \ldots (2.9)$$

$$\frac{\partial(\rho v)}{\partial t}+u\frac{\partial(\rho v)}{\partial x}+v\frac{\partial(\rho v)}{\partial y}=-\frac{\partial P}{\partial y}+\nabla.(\mu\nabla v)+S_v+\rho g\beta_T\left(T-T_{ref}\right) \qquad \ldots (2.10)$$

The laser welding of the dissimilar materials involves melting and solidification. Accordingly, the domain of interest consists of solid, liquid and solid/liquid interface. During welding, there is absence of flow in the domain of solid (where liquid fraction, $f_l=0$)

whereas flow develops in the liquid region (where liquid fraction $f_l = 1$) due to the thermal buoyancy, represented by the last term of the Eq. 2.10. The source terms, S_u and S_v as added in the momentum equations [74], provide an additional resistance to the flow in case of solid region whereas allows the melt to flow in case of liquid, and those are represented as

$$S_u = Au \quad \ldots (2.11a)$$

$$S_v = Av \quad \ldots (2.11b)$$

where *A* is defined as

$$A = -\frac{C(1-f_l)^2}{f_l^3 + b} \quad \ldots (2.12)$$

In the Eq.2.12, *C* is known as a morphological constant and usually assigned by a sufficiently large value of about 1.6×10^6. In the Eq.2.12, the term '*b*' is known as a computational constant included in respective model in order to avoid division of any value by zero during iterations. Based on the equations (Eq. 2.11a,b and Eq. 2.12), a zero value to the additional resistance occurs to in case of liquid phase ($f_l = 1$), and it changes from zero to a very high value in case of solid phase ($f_l = 0$).

2.4.3 Conservation of Energy

The temperature distribution within the computational domain is predicted by using the energy conservation equation [71-75] and presented as

$$\frac{\partial(\rho C_p T)}{\partial t} + u\frac{\partial(\rho C_p T)}{\partial x} + v\frac{\partial(\rho C_p T)}{\partial y} = \nabla.(k\nabla T) + S_h \quad \ldots (2.13)$$

In Eq. 2.13, S_h is a source term represents absorption and evolution of the latent heat during melting or solidification, respectively, of the weld materials. Based on assumptions, the latent heat source term (S_h) is presented [76] here as

$$S_h = \frac{\partial(\rho \Delta H)}{\partial t} \quad \ldots (2.14)$$

where ΔH is the enthalpy value varies as

$$\Delta H = 0 \; when \; T < T_{melt} \text{ (solid region)}$$

$$\Delta H = L_a \; when \; T > T_{melt} \text{ (liquid region)}$$

The enthalpy value (ΔH) is updated based on the enthalpy update scheme [71-77] in each of iterations during simulation. The enthalpy update scheme [71-78] is presented as Eq. 2.15.

$$[\Delta H_P]^{n+1} = [\Delta H_P]^n + \frac{a_P}{a_P^0}\lambda\left[\{H_P\}^n - C_p F^{-1}\{\Delta H_P\}^n\right] \quad \ldots (2.15)$$

In Eq. 2.15, ΔH_P is the latent heat content at the P^{th} node point of the respective computational domain, n is the present iteration number, a_P is the coefficient of T at the P^{th} node, and $a_P^0 = \rho\left(\frac{\Delta V}{\Delta t}\right)$. λ is a relaxation factor in the discretized energy equation, C_p is the specific heat of the materials, and F^{-1} is an inverse latent heat function equals to T_{melt} in the present case. After predicting the latent heat content (ΔH) in each of the nodes, the fractions of liquid and solid at any node in the computational domain are calculated as

$$f_l = \frac{\Delta H}{L_a} \quad \ldots (2.16a)$$

$$f_s = 1 - f_l \quad \ldots (2.16b)$$

2.4.3 Boundary Conditions

The laser welding process involves generation of the high energy density while applying the laser beam into the work pieces, and subsequent rise in the temperature is also very high. Under such a condition, consideration of combined convective and radiative heat transfers is suitable for all the bare surfaces. The heat transfer from any of the surfaces is considered as

$$q_S = (h_c + h_r)(T - T_a) \quad \ldots (2.17)$$

where h_c and $h_r = \varepsilon\sigma(T + T_a)(T^2 + T_a^2)$ are the convective and radiative heat transfer coefficients, respectively. ε is emissivity of surfaces, σ is the Stefan-Boltzmann constant, and T_a is the ambient temperature. The bottom surface is considered here as an adiabatic surface. Also an adiabatic condition is considered over the area of direct laser impingement.

2.5 Numerical Modelling

The present set of mass, momentum and energy conservation equations is coupled with the boundary conditions, and discretized based on the pressure based semi implicit finite volume method according to the SIMPLER algorithm as described by Patankar [79]. To establish a suitable spatial discretization and the levels of iteration convergence criteria, a comprehensive and complete grid-independence study is carried out. During simulation, the convergence is declared when $|(\phi - \phi_{old})|_{max} < 10^{-5}$ where ϕ stands for the solved variables at a grid point at the current iteration level, ϕ_{old} represents the corresponding value at the previous iteration level and ϕ_{max} is the maximum value of the variable at the current iteration level in the entire domain. The work conducts a comprehensive grid-independence study. It is found that a 82×42 uniform grid set is suitable for the present simulation and a time step of 0.01s offers a better convergence.

2.6 Closure

The present numerical investigation involves predicting of the transport phenomena while melting and solidification of weld materials in laser processing to prepare a weld joint. An appropriate mathematical model is considered in this chapter. The set of governing equations is solved using the Pressure based Finite Volume Method based on TDMA algorithm. In the model, the enthalpy update scheme is used to trace the solid/liquid interface during melting and solidification.

References

[51] P. S. Ghosh, A. Sen, S. Chattopadhyaya, S. Sharma, J. S. Chohan, R. Kumar, S. Singh, and A. Joshi, "Numerical investigation of thermal residual stress distribution for the sustainability of laser welded joints of dissimilar materials", *Materials Today: Proceedings*, Vol. 68 (2022), A16–A21

[52] K. Martinsen, S. J. Hu, and B. E. Carlson, "Joining of dissimilar materials, *CIRP Annals-Manufacturing Technology*, Vol. 64 (2) (2015), pp. 679–699.

[53] Z. Sun, Joining dissimilar material combinations: materials and processes, *Int. J. Mater. Prod. Technol.*, Vol. 10 (1–2) (1995), pp. 16–26

[54] T. F. Song, X. S. Jiang, Z. Y. Shao, Y. J. Fang, D. F. Mo, D. G. Zhu, and M. H. Zhu, Microstructure and mechanical properties of vacuum diffusion bonded joints between Ti-6Al-4V titanium alloy and AISI316L stainless steel using Cu/Nb multi-interlayer, *Vacuum*, Vol. 145 (2017), pp. 68–76

[55] F. Impero, F. Scherillo, A. Astarita, K. A. Beamish, M. Curioni, A. Squillace, and X. R. Zhou, Study of the Metallurgy of a Dissimilar Ti-6Al-4V–Stainless Steel Linear Fiction Welded Joints, *Key Engineering Materials*, *Trans Tech Publications Ltd.*, Vol. 651 (2015), pp. 1427-1432

[56] J. L. Murray, The Fe-Ti (iron-titanium) system, *Bulletin of Alloy Phase Diagrams*, Vol. 2 (3) (1981), pp. 320–334

[57] ASM Aerospace Specification Metals, Inc.; Florida. https://asm.matweb.com/search/SpecificMaterial.asp?bassnum=mtp641

[58] P. Tan, F. Shen, B. Li, and K. Zhou, A thermo-metallurgical-mechanical model for selective laser melting of Ti6Al4V, *Materials & Design*, Vol. 168 (2019), 107642

[59] Z. Yan, W. Liu, Z. Tanga, X. Liu, N. Zhang, Z. Wang, and H. Zhang, Effect of thermal characteristics on distortion in laser cladding of AISI 316L, *Journal of Manufacturing Processes*, Vol. 44 (2019), pp. 309-318

[60]https://www.matweb.com/search/datasheet_print.aspx?matguid=1336be6d0c594b55afb5ca8bf1f3e042

[61] P. Ansari, A. U. Rehman, F. Pitir, S. Veziroglu, Y. K. Mishra, O. C. Aktas, and M. U. Salamci, Selective Laser Melting of 316L Austenitic Stainless Steel: Detailed Process Understanding Using Multiphysics Simulation and Experimentation, *Metals*, Vol. 11 (2021), 1076

[62] T. Kik, Heat Source Models in Numerical Simulations of Laser Welding, *Materials*, Vol.13 (2020), 2653

[63] P. R. F. Teixeira, D. B. Araújo, and L. A. B. Cunha, Study of the Gaussian Distribution Heat Source Model Applied to Numerical Thermal Simulations of TIG Welding Processes, *Ciência & Engenharia (Science & Engineering Journal),* Vol. 23 (1) (2014), pp.115–122.

[64] Mickael Courtois, Muriel Carin, Philippe Le Masson, Sadok Gaied and Mikhael Balabane, Study of A new approach to compute multi-reflections of laser beam in a keyhole for heat transfer and fluid flow modelling in laser welding, *J. Phys. D: Appl.Phys*., Vol. 46(2013), 505305(1-14)

[65] J. F. Helgaker, and T. Ytrehus, Study of coupling between Countinuity/Momentum and Energy Equation ID Gas Flow, Energy Procedeia, Vol. 26(2012), pp. 82-89.

[66] R. Rai, J. W. Elmer, T. A. Palmer and T. D. Roy, Study of heat transfer and fluid flow during keyhole mode laser welding of tantalum, Ti-6AI-4V, 304L staninless steel and vanadium, *J. Phys. D: Appl Phys*., Vol. 40 (2007), pp. 5753-5766.

[67] G. Phanikumar, K. Chattopadhyay , Pradip Dutta, Modelling of transport phenomena in laser welding of dissimilar metals, *International journal of Numerical Methods for Heat and Fluid Flow*, Vol.11 (2), pp. 156-174

[68] A. Karimipour, E. Abedini, H. Ajam, S. M. H. Sarvari, Modelling of fluid and laser welding with a heat source, Advanced Materials Resaearch, Vols. 622-623(2013), pp. 618-622

[69] P. R. Chakraborty, Study of enthaply porosity model for melting and solidification of pure-substances with large difference in phase specific heats, *International Communications in Heat and Mass Transfer*, Vol. 81(2017), pp. 183-189

[70] N. Pathak, A. Kumar, A. Yadav, and P. Dutta, Study of effects of mould filling on evolution of the solid- liquid interface during solidification, *Appiled Thermal Engineering*, Vol. 29(2009), pp.3669-3678

[71] B. Mendez, and A. Velazquez, Study of finite point solver for the simulation of 2-D laminar incompressible unsteady flows, *Comp. Methods Appl. Mech. Engg.*, Vol.193(2004), pp. 825-848.

[72] J. L. Guermond, and L. Quartapelle, Study of a Projection FEM for Variable Density Incompressible Flows, *Journal of Computational Physics,* Vol.165 (2000), pp.167-188

[73] S. Ganesan, and D. R. Poirier, Study of conservation of mass and momentum for the flow of interdendritic liquid during solidification", *METALLUIRGICAL TRANSACTION B*, Vol. 21B(1990), 173

[74] G. Wei, J. T. Kirby, and A. Sinha, Study of generation of waves in Boussinesq models using a source function method, *Coastal Engineering*, Vol. 36(1999), pp.271-299

[75] R. Kumar , and S. Lomash, Study of Enhancement of Temperature Distribution Heat Transfer Coeffcient of Ribbed Tube by Simulation, *ISSN: 2582-4600*.

[76] Y. Huang, Q. Han, and X. Liu, Study of experimental investigation on the melting and solidification performance enhancement of a fractal Latent heat storage unit, *International Journal of Heat and Mass Transfer*, Vol.179 (2021 121640.

[77] S. Chakraborty and P. Dutta, Study of a Generalized Formulation for Evaluation of Latent Heat Function in Enthalpy-Based Macroscopic Models for Convection-Diffusion Phase Change Processes, *Metallurgical and Materials Transactions B*, Vol. 32 (3), pp. 562-564

[78] P. R. Chakraborty and P. Dutta, Study of a Generalised Enthalpy Update Scheme for Solidification of a Binary Alloy with Solid Phase Movement, Metallurgical and Materials Transactions B: Process Metallurgy and Materials Processing Science, Volume: 42 (6) (2011), pp.1075 – 1079

[79] Patankar, S.V. (1980) Numerical heat transfer and fluid flow. Hemisphere Publishing Corporation. New York.

Chapter-III

Results and Discussion

3.1 Introduction

The transport phenomena during laser beam welding of dissimilar materials are presented in this chapter. This includes consideration of a suitable problem and modeling of the problem using the mass, momentum and energy equations with the relevant source terms. Further modeling of the laser source and boundary conditions are also considered properly in order to model the problem effectively. This work then considered the numerical study based on the finite volume method (FVM) and development of a code on FORTRAN platform. Initially, validation of the developed code is considered and subsequent it involves prediction of results: temperature distribution, area of HAZ, penetration depth, weld-bead geometry under different process parameters.

3.2 Development of a FORTRAN based numerical code along with setting of the proper boundary conditions, and necessary validation of the developed code

This work includes numerical simulation of a laser welding process in order to understand the transport phenomena during joining of two dissimilar materials, i.e., Ti-6Al-4V titanium alloy

and AISI 316L stainless steel in the present thesis. Accordingly, a numerical code is developed on the FORTRAN platform. The numerical code is developed based on the finite volume method considering the SIMPLER algorithm includes using of the power law scheme and the staggered grids for velocity vector, and the subsequent solution of finally obtained discretized simultaneous equations is performed on the TDMA algorithm. The setting of boundary conditions plays an important role in the present problem as the whole generated heat of the laser is transferred to the ambient through convection and radiation only that is represented here by an equivalent heat transfer coefficient. Hence, an emphasis is drawn on inclusion of the boundary conditions within the code. Accordingly, a simple slab of Ti-6Al-4V titanium alloy with thickness of 80mm is considered for validation of the code where the initial temperature of the slab and heat transfer coefficient related to the ambient fluid are considered as 1632 °C and 20 W/m^2-°C. Other thermo-physical properties are considered from the Table 2.1. The variation of temperature with time at centre of the slab is presented in the Fig. 3.1, and compared it with that available as the standard solution in the book of heat transfer by Ozisik (1984). A very good agreement is found between the numerical and analytical solutions. The developed code is then tested for necessary grid independent study. A rigorous grid independent study is conducted considering different values of uniform grids (n_xxn_yxn_z) such as 72x72x32, 82x82x42, 92x92x52, 102x102x62, 122x122x62 and 142x142x62. The variation of the central temperature with time is presented in Fig. 3.2. Hence, based on the analysis, a suitable grid structure of 82x82x42 is selected for the present study. The code is then extended for the present numerical analysis.

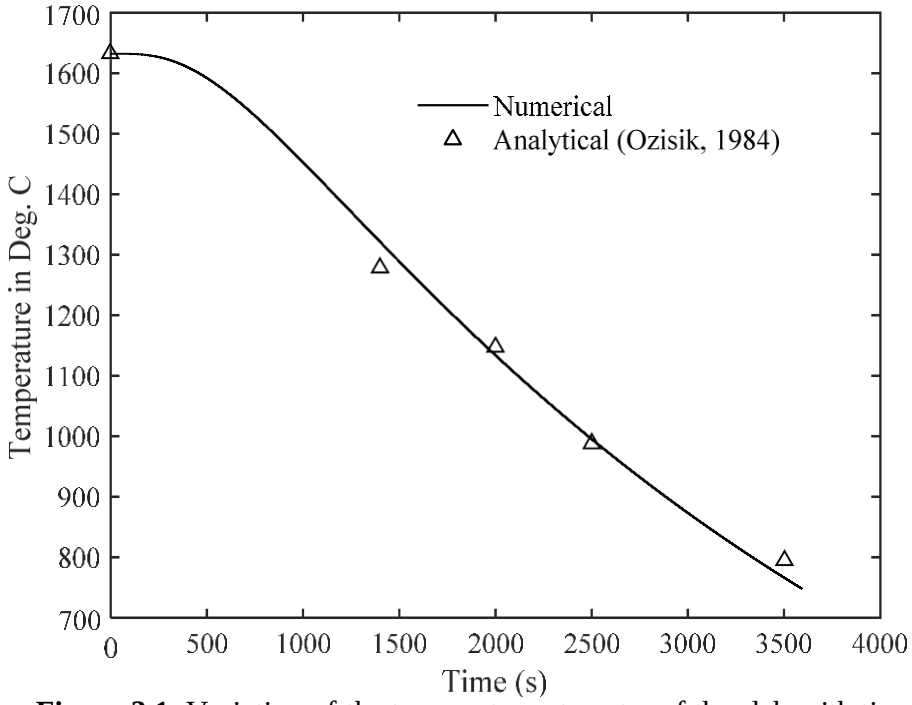

Figure 3.1: Variation of the temperature at centre of the slab with time

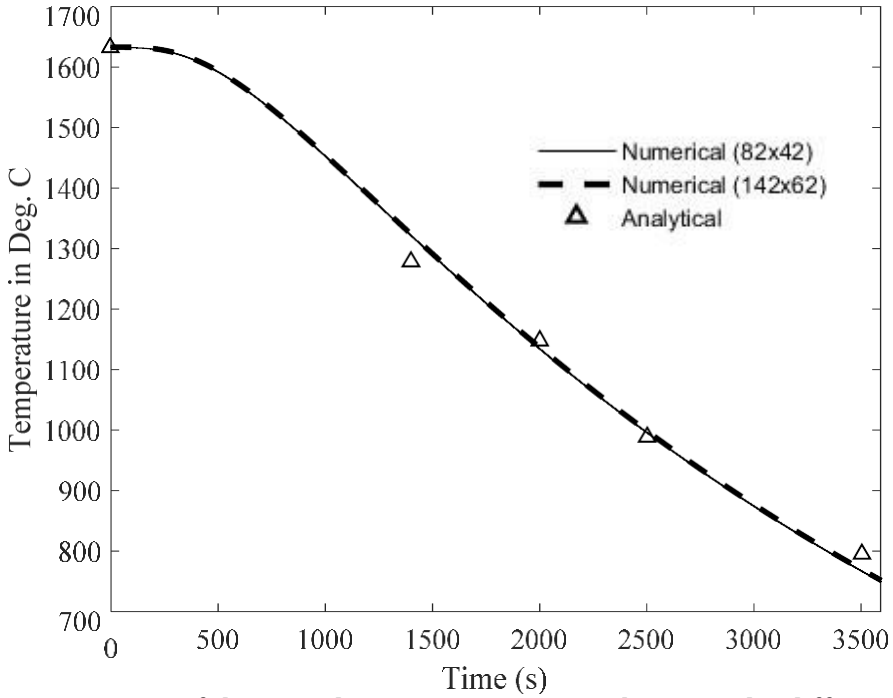

Figure 3.2: Comparison of the central temperatures vary with time under different grid structures

3.3 Representation of the laser beam as a volumetric heat source in the numerical code

In the present thesis, a 3D conical heat source with a Gaussian distribution is considered, and the related parameters are presented in the Table 3.1. Referring to the Fig. 2.3, the beam radius (r_0) decreases linearly as thickness of the material increases [62], and is represented as

$$r_0 = r_l + (r_u - r_l)\frac{(z - z_l)}{(z_u - z_l)} \quad \ldots (3.1)$$

where r_u and r_l are the upper and lower beam radii, and the upper and lower z-coordinates are z_u and z_l, respectively. The volumetric energy (W/m^3) distribution as per the Gaussian curve is considered as

$$Q(x,y,z,t) = Q_0 \exp\left(\frac{-3[(x-x_c)^2 + (y-y_c)^2]}{r_0^2}\right) \quad \ldots (3.2)$$

In the present thesis, a modified introduced distributed volumetric heat source (Q_0, W/m^3) of the laser beam is considered in order to present its realistic value as

$$Q_v - \frac{9\eta P e^3}{1000\pi(e^3-1)(z_u - z_l)(r_u^2 + r_l^2 + r_u r_l)} \quad \ldots (3.3)$$

For verification of the present heat source model, the dimensions of the concerned computational domain are incorporated in the code, and identified separate domains for the dissimilar materials or work pieces. Then, all the thermo-physical properties of the work pieces as per the Table 2.1 are incorporated in the numerical code. Then, the peak temperature for

different values of the laser power is predicted as function of the time as shown in the Fig. 3.3. It is found that the peak temperature achieves within 0.14s to 0.18s. Corresponding variation of the peak temperature with laser power is presented in the Fig. 3.4 and compared with those predictions by Mohan *et al*. [80]. A good agreement of the present model is found as shown in the Fig. 3.4, without incorporation of the melting and solidification phenomena of the materials, and considering the related boundary conditions. Then, the modified heat source model is extended for further study of the laser welding process.

Table 3.1: The laser parameters for the 3D model [62]

Description of the parameters	***Value***
Type of laser	Argon
Laser power (*P, W*)	--
Beam radius (*m*)	125
Upper radius of the heat source (r_u, *m*)	734
Lower radius of the heat source (r_l, *m*)	356
Process efficiency ( )	0.45
Welding speed (*v, m/min*)	--
Thickness of the work piece (*mm*)	4
Upper z-coordinate (z_u, *m*)	4000
Lower z-coordinate (z_l, *m*)	0
e	2.7182818
	3.14159265358979

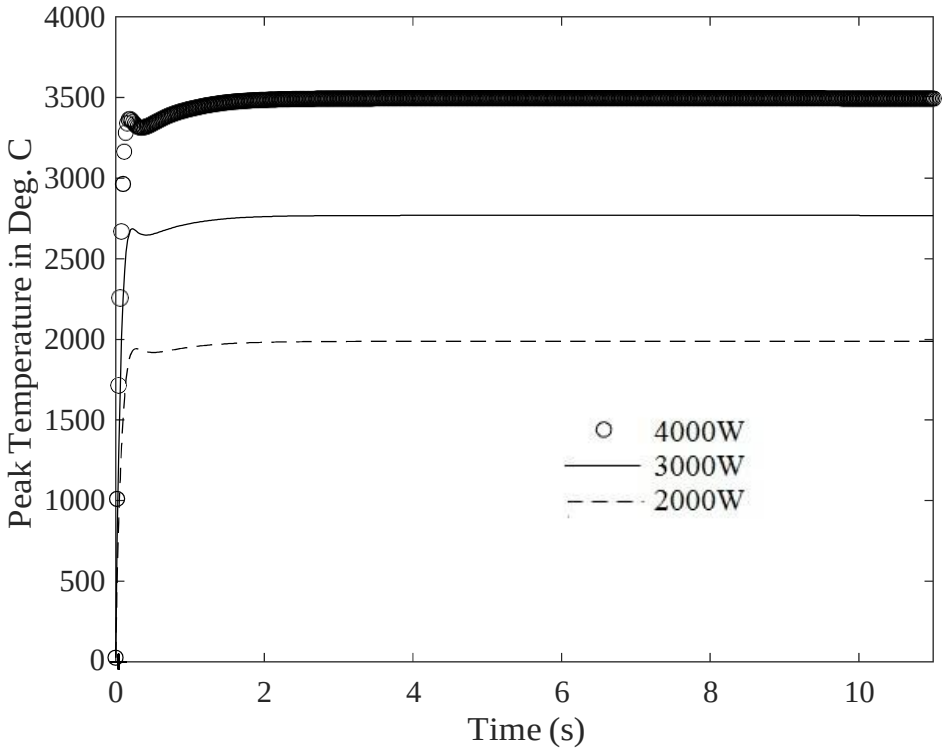

Figure 3.2: Variation of peak temperature with time for different values of the laser power

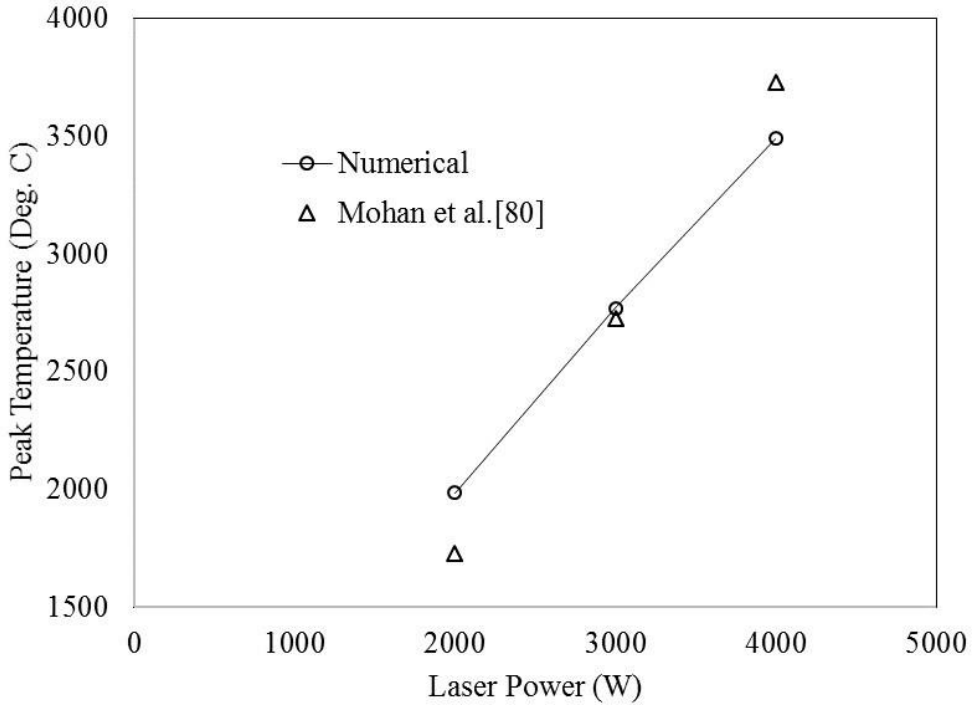

Figure 3.3: Comparison of the peak temperature at different values of the laser power

3.4 Study of the transport phenomena during welding of the work pieces with stationary laser beam

In this case, a stationary heat source is considered to represent a laser power of 3000W. The other thermo-physical properties for the concerned dissimilar materials are considered as per the Table 2.1. The dimensions for the cross section (the computational domain) of the weld materials are considered as 80mm×4mm with a grid size of 82×42. The necessary boundary conditions are presented in the Chapter-II. Fig. 3.4 represents corresponding distribution of the heat source in the computational domain. A maximum value of about 272.89×10^6 W/m^3 is found on top of the domain whereas a minimum value of about 2.95×10^6 W/m^3 is found at bottom of the domain. Application of the high density laser source increases the temperature of the weld materials and melts the materials at a temperature about of their melting temperatures. Accordingly, in this present section, the temperature distribution along with the progress of melt-front is presented with time. Fig.3.5 (a) represents the distribution of temperature with melt-front at time 0.1s where top part of the domain is melted. The melting of the materials increases with time as shown in the Fig. 3.5 (b, c), and the melt-front reaches to the bottom of the domain at about1.0s as shown in the Fig. 3.5(d) and the Fig. 3.6 presents the melt-front at 1:1 scale with a weld-pool of about 4mm wide. Corresponding increase of the melt fraction in the domain with time is shown in the Fig. 3.7. It is found that melt fraction reaches to 1 within a considered domain (about 7mm wide is considered here at middle of the computational domain) at 1.08s, which also represents reaching of the melt-front at bottom of the domain. This work is then considered removal of the heat source after reaching of the melt-front at bottom of the domain in order to understand the solidification behaviour of the melted weld materials. Both the convection and radiation from the bare surfaces reduce temperature of the melt that starts solidifying from top of

the domain. The corresponding melt-front moves downwards as shown in the Fig. 3.5 (e, f). Complete solidification of the melt takes place at 2.86s as shown in the Fig. 3.7. Hence total time for melting is 1.08s and that for the solidification is 1.78s.

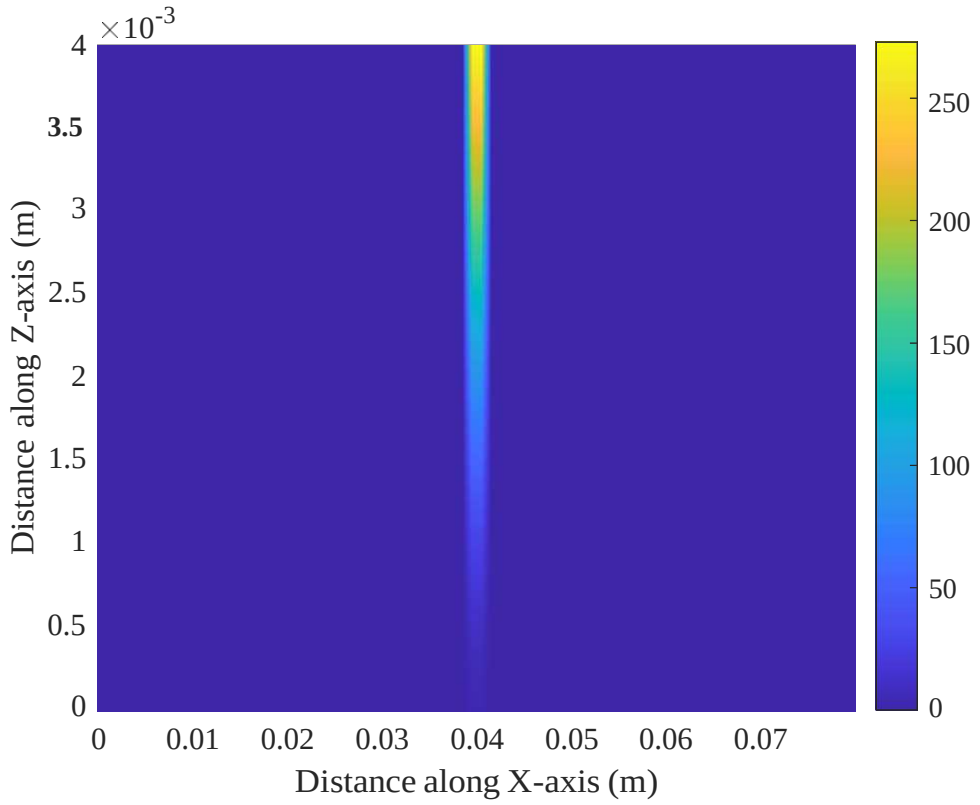

Figure 3.4: Distribution of volumetric laser heat source ($\times 10^6$ in W/m^3) for P=3000W

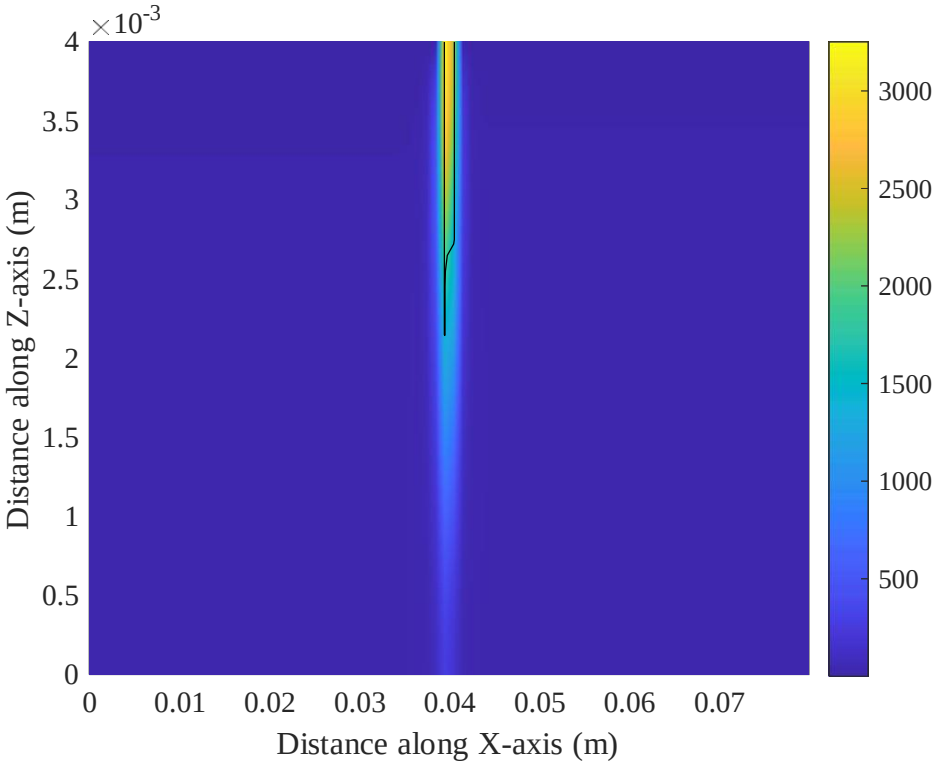

Fig. 3.5(a)

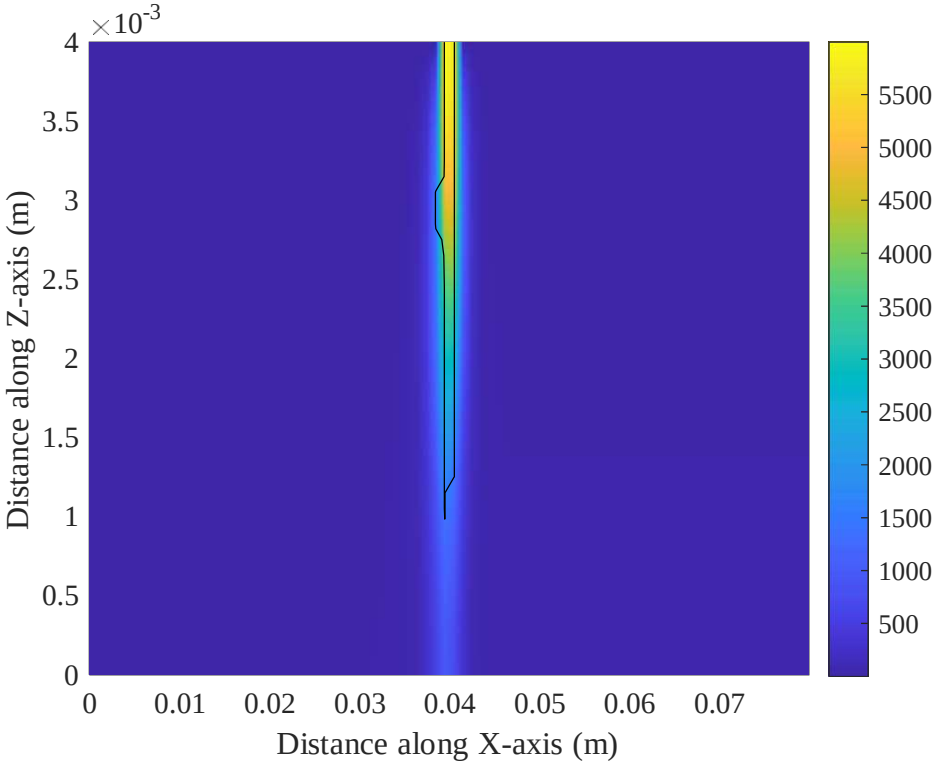

Fig. 3.5 (b)

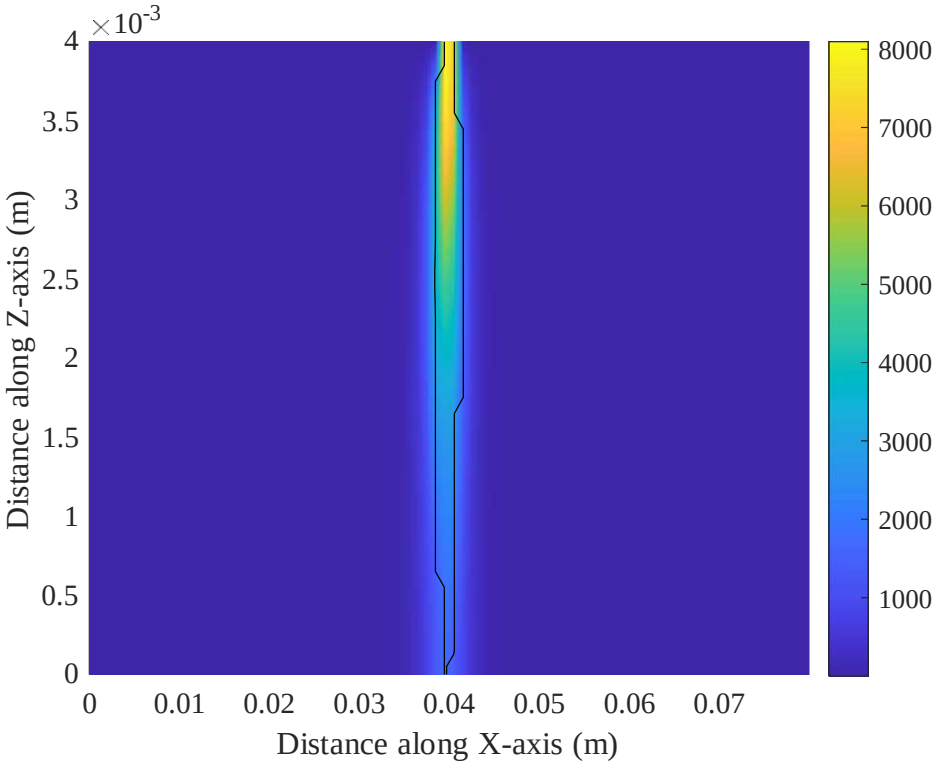

Fig. 3.5 (c)

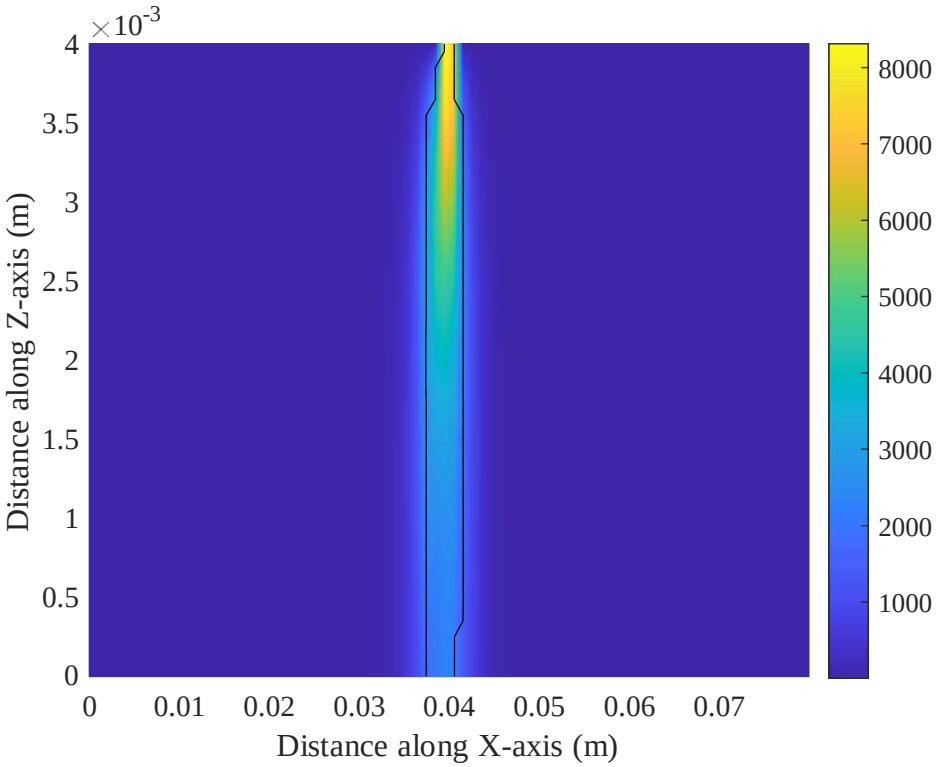

Fig. 3.5 (d)

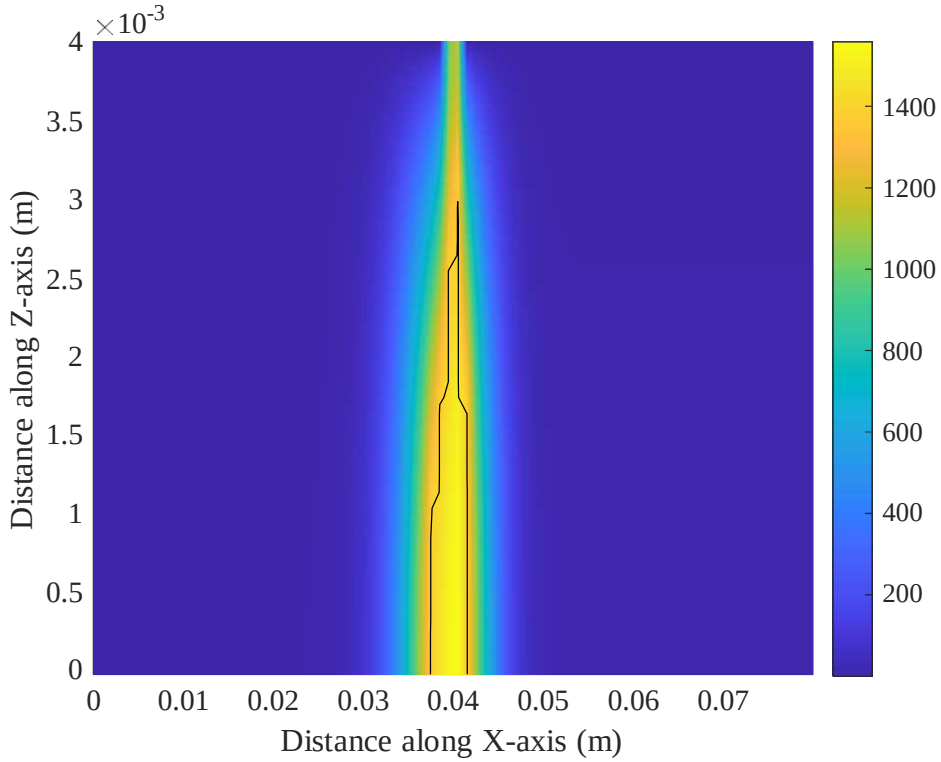

Fig. 3.5 (e)

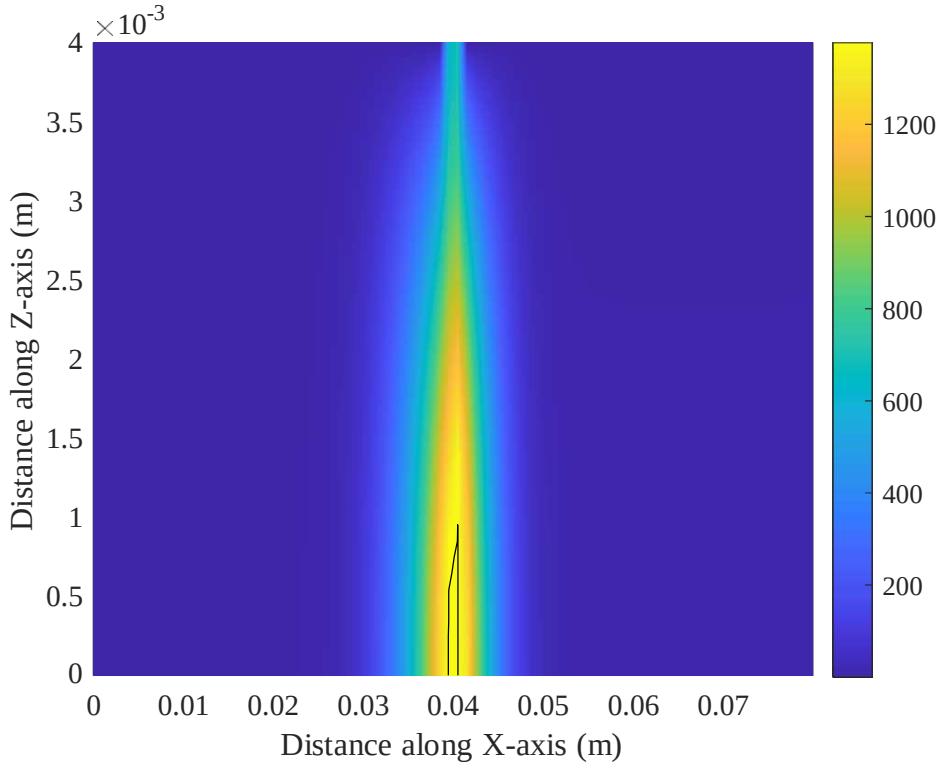

Fig. 3.5 (f)

Figure 3.5: Distribution of temperature and subsequent tracking of the melt-front with time for P=3000W: (a) 0.1s, (b) 0.3s, (c) 0.6s, (d) 1.0s, (e) 2.0s, and (f) 2.5s

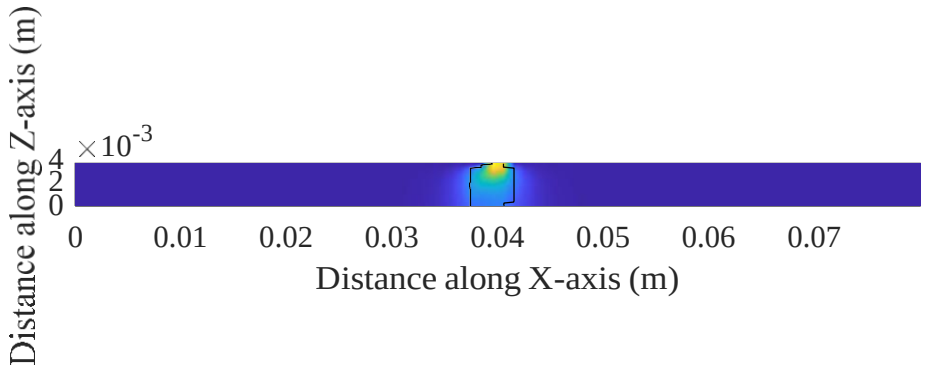

Figure 3.6: Presenting the melt-front at 1:1 scale at the time of 1.0s for P=3000W

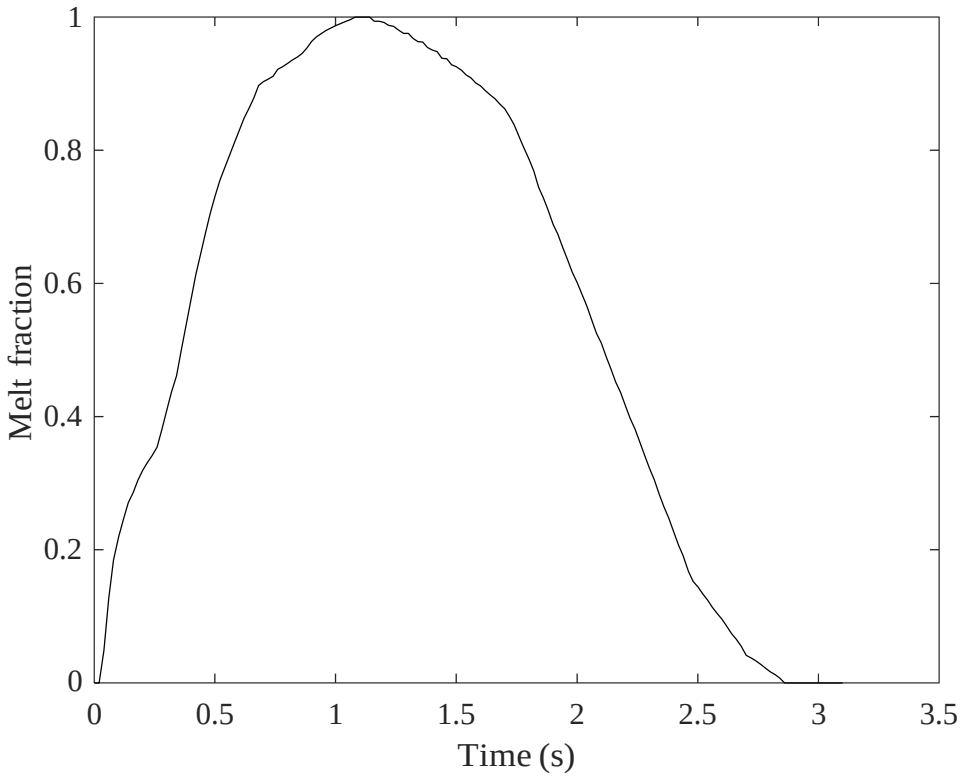

Figure 3.7: Presence of the melt fraction with time for P=3000W

This work also considered the visualization of fluid flow in the melt during welding of dissimilar materials due to thermal buoyancy only. Analyzing the Table 2.1, it is found that the thermal expansion coefficient of the AISI 316L is high and melting temperature is low that implies high ΔT compared to the Ti-6Al-4V, those result a high bouyancy force in case of AISI 316L. It is mention here that the ratio of thermal expansion coefficient between AISI 316L and Ti-6Al-4V is 2.2 where as density ratio is 1/1.76. Hence, the effect of the thermal expansion coefficient is more prominent than the density of the material. Thus, the high buoyancy induces moving of the fluid from AISI 316L to Ti-6Al-4V. Fig. 3.8 shows the corresponding loop of the flow using streamlines and its sub-figure shows the direction of flow at top of the domain. Due to this melt flow, mixing of the materials is possible.

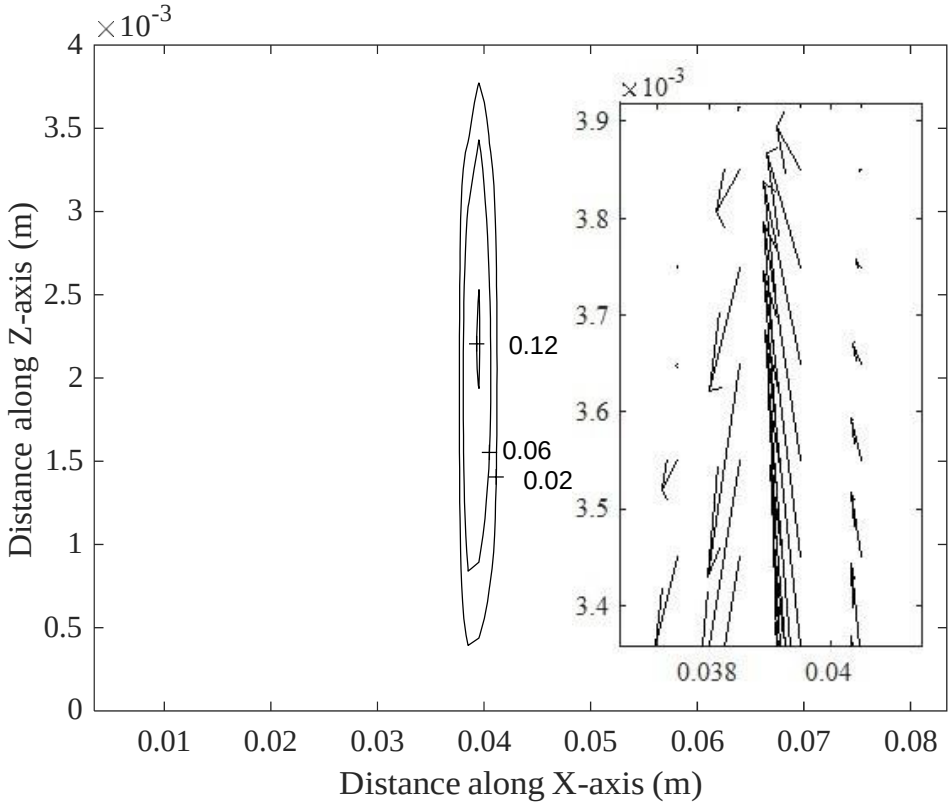

Figure 3.8: Streamline and velocity vector at a time of 1.0s for P=3000W

Further, it is an important issue to identify the heat affected zone (HAZ) during the laser welding due to application of a high density energy source. The high temperature developed during the welding results transformation of the phases in the solid state too at above of the recrystallization temperature which is in between 800 C and 850 C for both of the materials. In the present case, 825 C is considered to identify the heat affected zone (HAZ). Corresponding evolution of the HAZ with time is shown in the Fig. 3.9. It is about 6mm wide at 1.0s as found in the Fig. 3.9(b). The HAZ is wider at later stage of the solidification as found in the Fig. 3.9(c) possibly due to evolution of the latent heat during solidification.

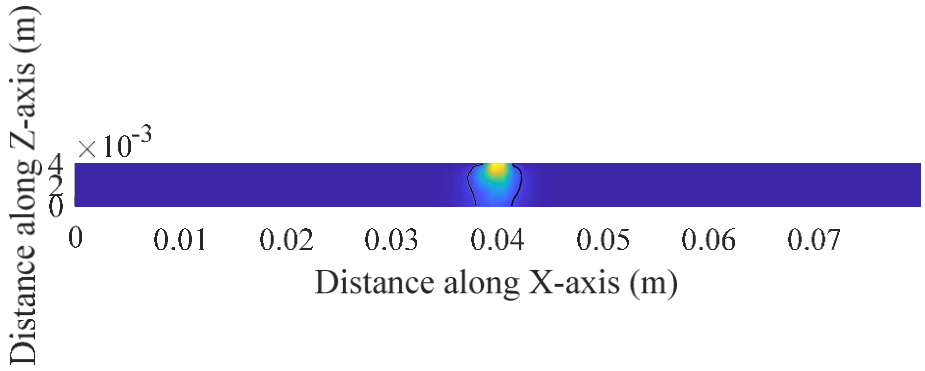

Fig. 3.9 (a)

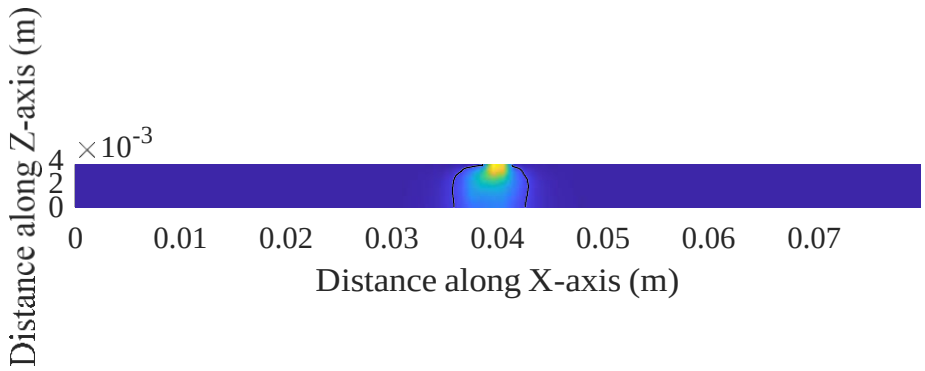

Fig. 3.9 (b)

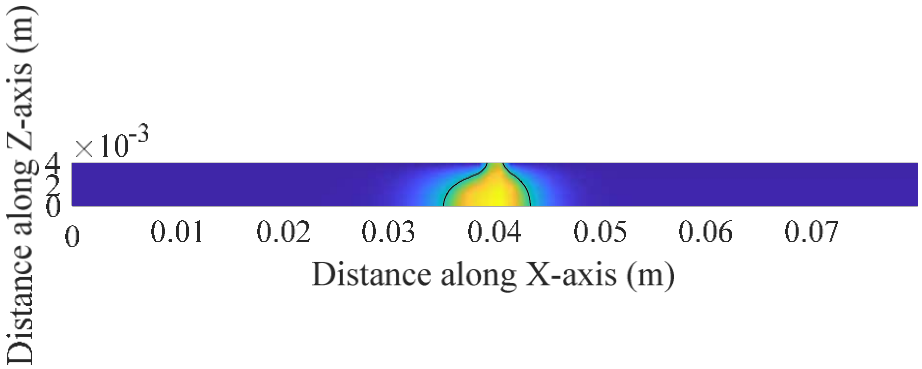

Fig. 3.9 (c)

Figure 3.9: Evolution of heat affected zone (HAZ) with time for P=3000W: (a) 0.5s, (b) 1.0s, and (c) 2.0s

In order to understand the behaviour of the melting and solidification under different values of the laser power, a parametric study is also considered in this work subsequently. Five different values (1000W, 2000W, 3000W, 4000W, and 5000W) of the laser power are considered. Fig. 3.10 shows values of the corresponding volumetric heat source representing the laser beam at top and bottom surfaces of the weld for laser powers. A sharp increase in the volumetric heat source is found in case of top surface of the weld with increase in laser power whereas the effect of laser power on bottom surface of the weld is less. Then under different values of the laser power, the total time to melt the materials across depth of the weld, and total time to solidify the molten materials are predicted. Fig. 3.11 shows corresponding melting and solidification times under different laser powers. The melting time decreases with increase of the laser power. The higher laser power melts the materials more, accordingly width of the weld-pool increases as shown in the Fig. 3.12. Similarly, at a higher laser power, the HAZ is also increases as shown in the Fig. 3.12. Now, the more melt or molten metal at high laser power needs more time to solidify completely. Accordingly, the solidification time of molten materials increases with laser power as shown in the Fig. 3.11.

In the laser welding, the travelling speed of the laser is an important parameter to control the properties of the weld. Hence, considering width of the weld-pool and total meting time to melt the materials across depth of the weld, a limit to the travelling speed of laser is calculated ensures melting of the materials across depth of the weld. The values of the limit to the travelling speed under different laser powers are presented in the Fig. 3.13. At a high laser power, a high limit to the traveling speed is allowable. However, in all above cases, the heating of the materials is considered from initial temperature; accordingly the limit may vary in case of travelling of the laser beam.

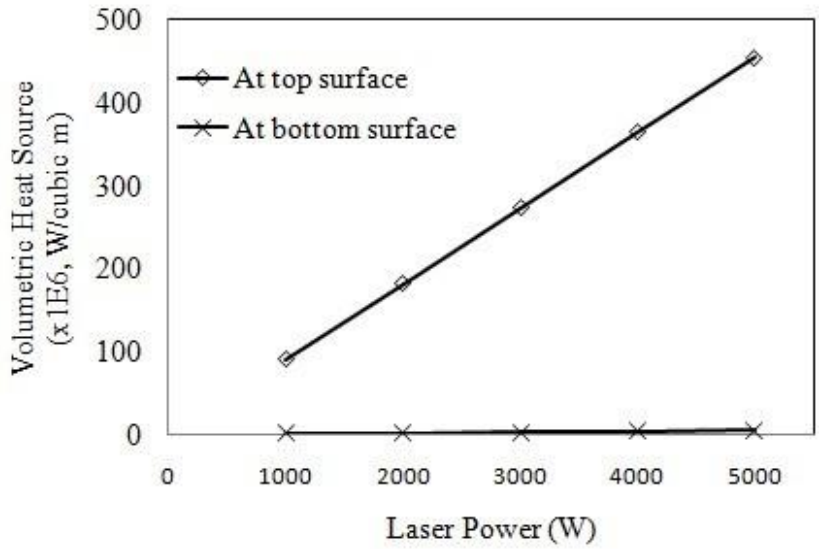

Figure 3.10: Typical values of the volumetric heat source corresponding to a laser power at top and bottom surface of the weld materials

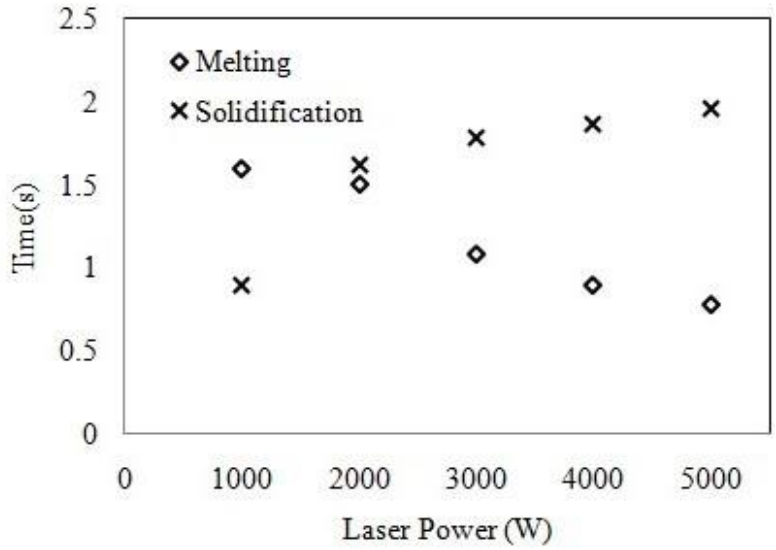

Figure 3.11: Total time to melt the materials across depth of the weld, and to solidify the molten materials for different values of laser power

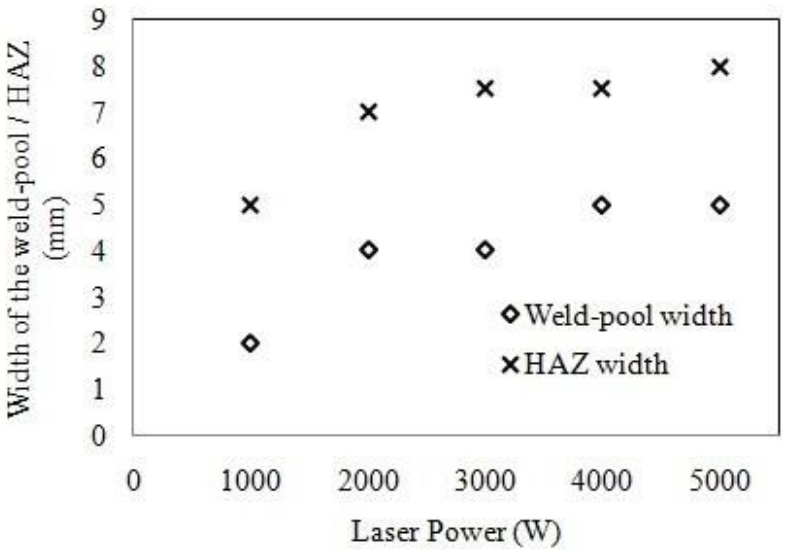

Figure 3.12: Width of the weld-pool and HAZ for different values of laser power

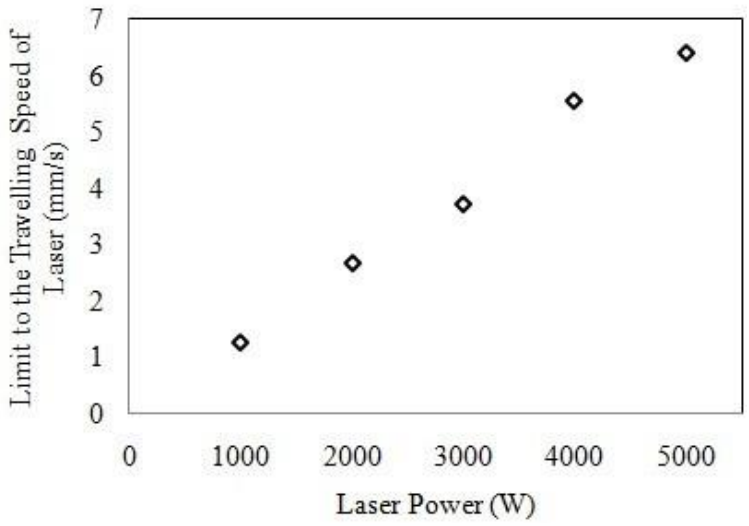

Figure 3.13: Maximum travelling speed of laser in order to melt the materials across depth of the weld for different values of laser power

3.5 Study of the transport phenomena during welding of the work pieces with travelling laser beam

It is recognized that both the travelling speed and power of laser beam play important role in the transport phenomena during welding of the materials. Hence, in this section, the transport phenomena are analyzed under different travelling speeds and powers of the laser beam. Fig. 3.14 represents the distribution of temperature and corresponding tracking of the melt-front for a laser power of 3000W under different travelling speeds (10mm/s, 10.5mm/s, 11mm/s, 12.5mm/s, and 15mm/s) of the laser beam in the part of Ti-6Al-4V (at middle of the weld in the *x*-direction) at a distance of 45mm along *y*-axis which is the travelling direction of the laser beam. It is obvious that, at lower travelling speed, the heating time is more. Accordingly, more melting of the materials is observed at lower travelling speed as found in the Fig. 3.14(a). With increasing the travelling speed, melting of the materials reduces and corresponding size of the weld-pool also reduces as found in the Fig. 3.14 (b to e). The depth of penetration reduces with increase in travelling speed of the laser beam, accordingly. In Fig. 3.15, the variation of depth of penetration

with travelling speed of the laser beam is shown for the laser power of 3000W at y = 45mm where the depth of penetration reduces with increase in travelling speed of the laser beam. Now, this depth of penetration depends on the power of the laser beam. Subsequent, the numerical simulation is extended for different laser powers. The corresponding variation of the depth of penetration with power of the laser beam is presented in Fig. 3.16. It is found that the depth of penetration increases with increase in the laser power due to high energy density at the high laser power. The all above presentations are considered for the part of Ti-6Al-4V. However, a comparison of that part is made with the part of AISI 316L for the laser power of 3000W at a travelling speed of 15mm/s at y=45mm as shown in Fig. 3.17. It is found that weld-pool size is smaller in case of AISI 316L. In the section 3.4, it is discussed that the high buoyancy induces in the part of AISI 316L than Ti-6Al-4V part. The high buoyancy is one of the reasons to enhance the heat transfer in the part of AISI 316L, and reduces the size of the weld-pool.

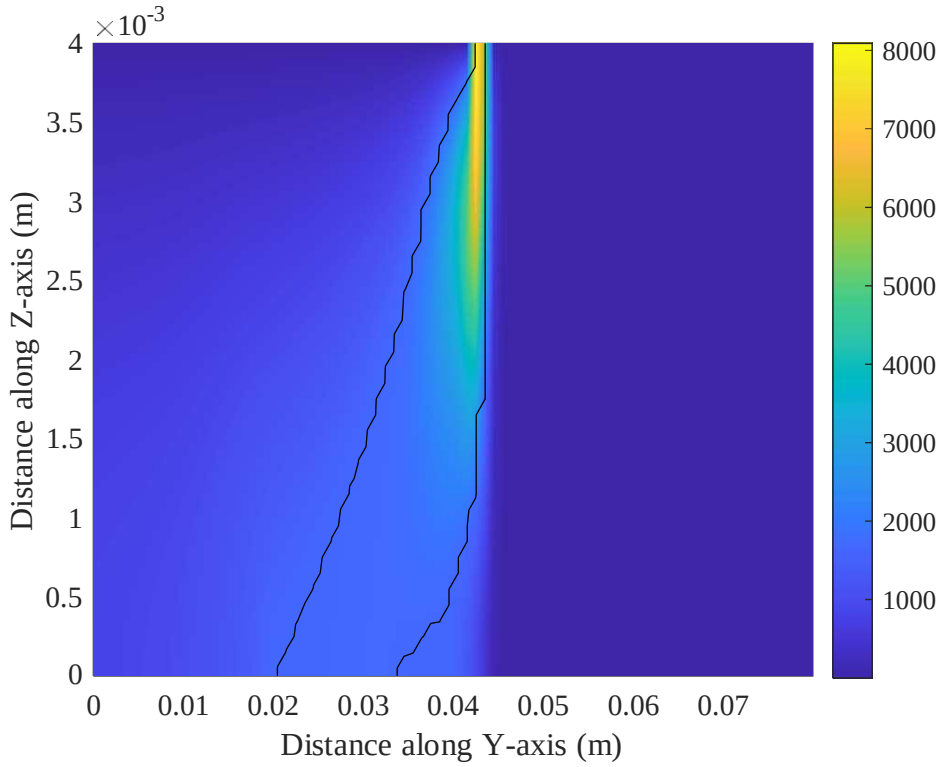

Fig. 3.14(a) uscan=10mm/s, t=4.5s

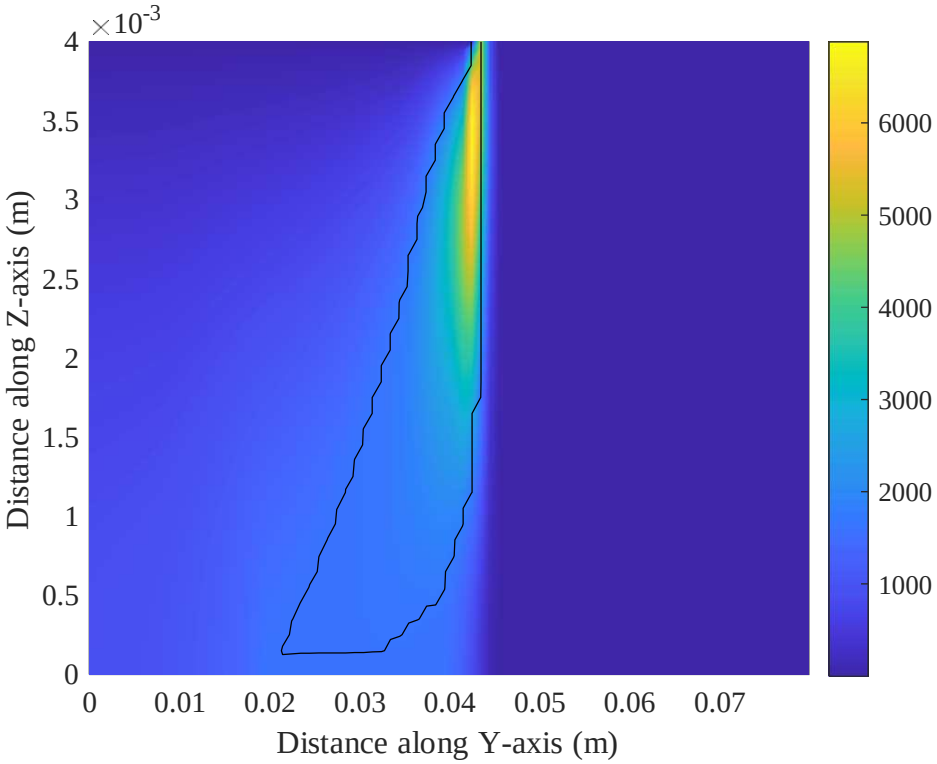

Fig. 3.14 (b) uscan=10.5mm/s, t=4.3s

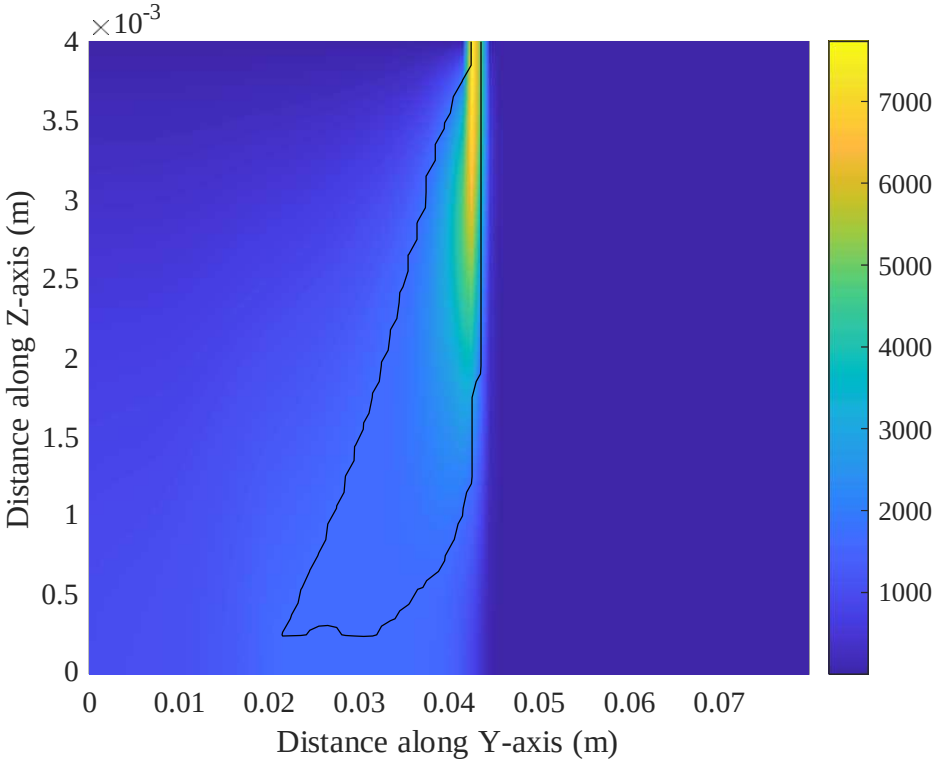

Fig. 3.14 (c) uscan=11mm/s, t=4.1s

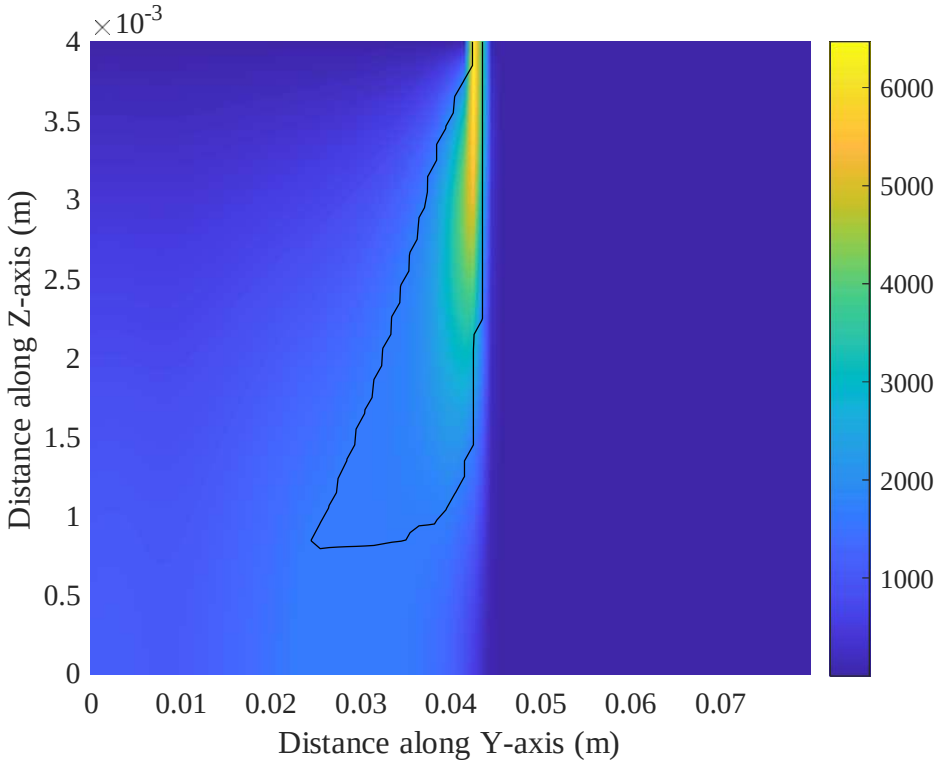

Fig. 3.14 (d) uscan=12.5mm/s, t=3.6s

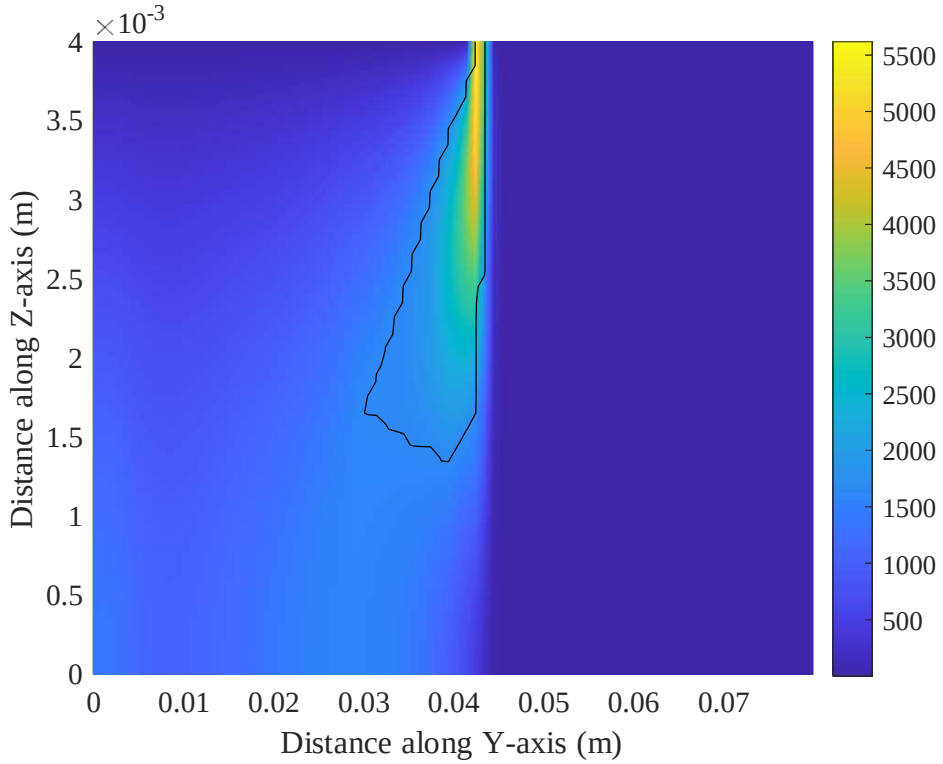

Fig. 3.14 (e) uscan=15mm/s, t=3.0s

Figure 3.14: Distribution of temperature and tracking of the melt-front for P=3000W under different travelling speeds (uscan) of the laser beam (in the part of Ti-6Al-4V)

[61]

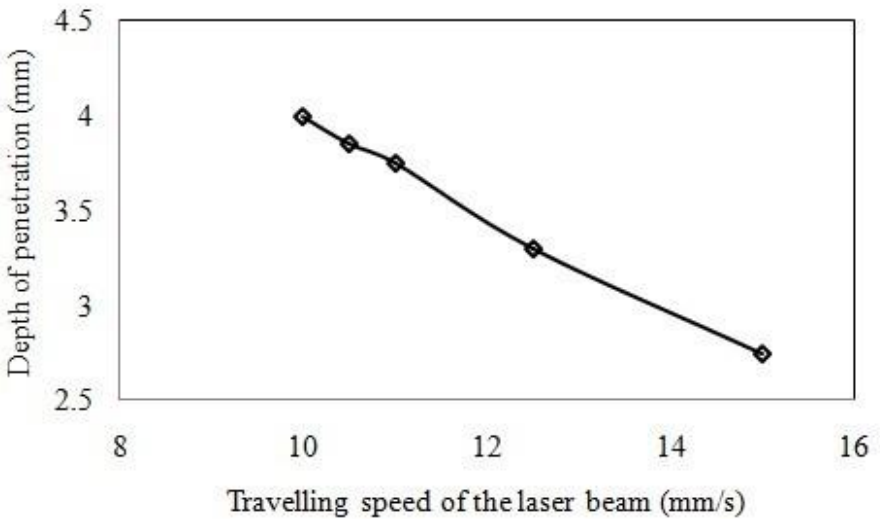

Figure 3.15: Variation of the depth of penetration with travelling speed of the laser beam for P =3000W at *y* = 45mm

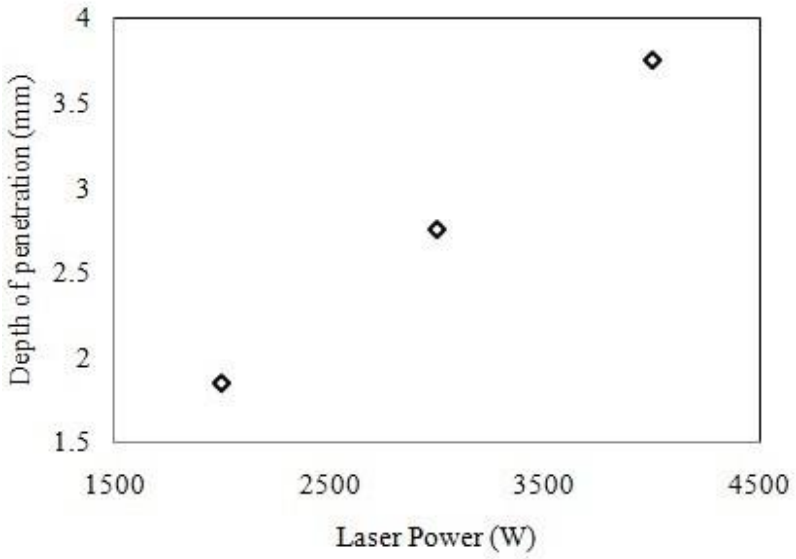

Figure 3.16: Variation of the depth of penetration for different laser powers at travelling speed of 15mm/s and *y* = 45mm

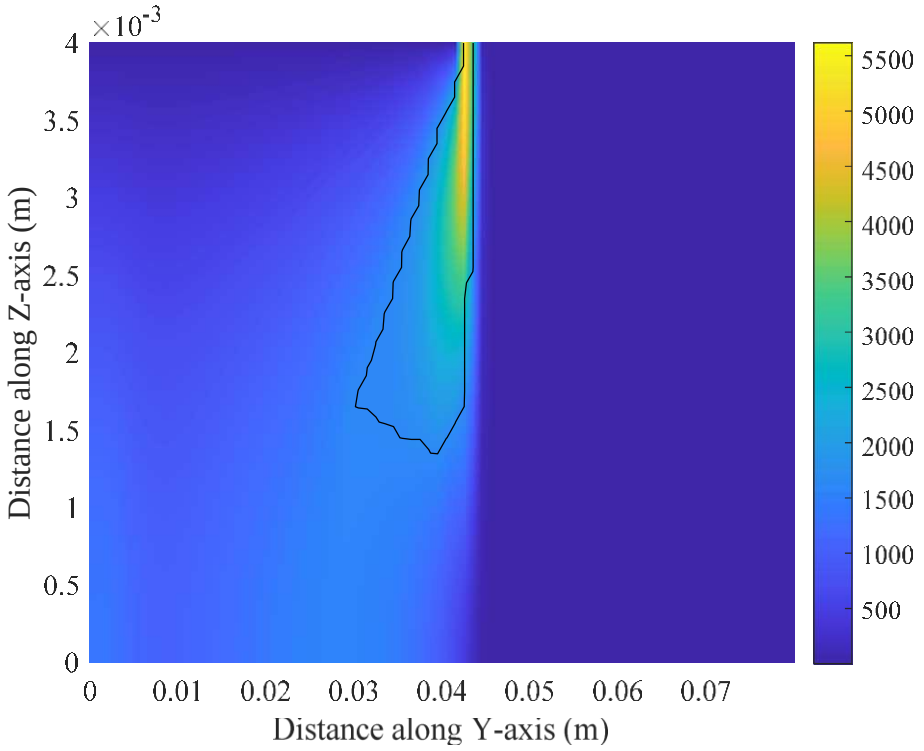

(a)

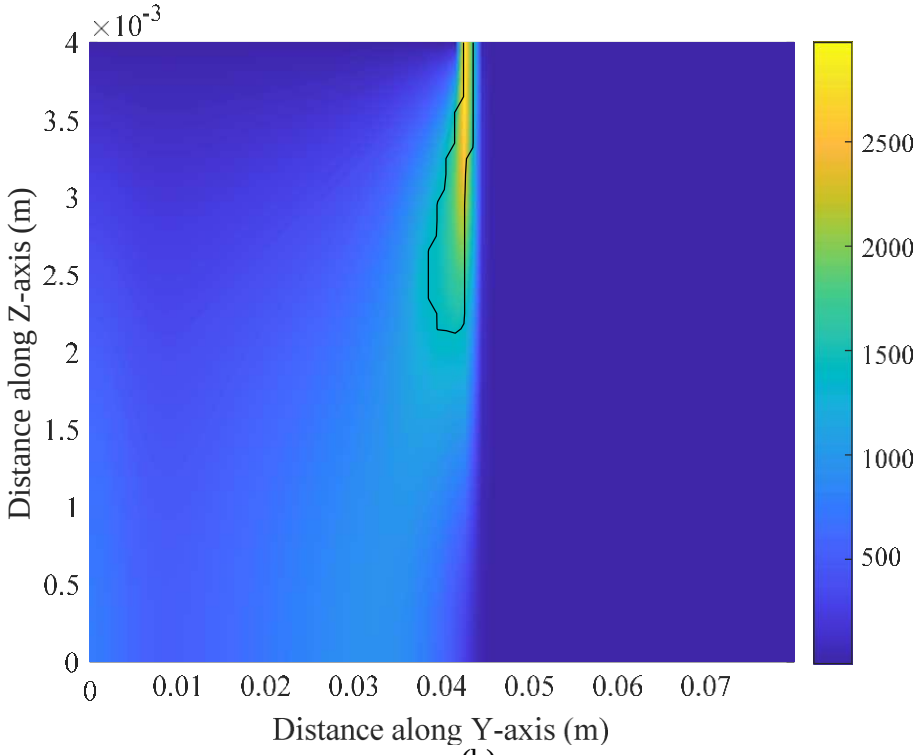

(b)

Figure 3.17: Distribution of temperature and tracking of the melt-front for P=3000W at a travelling speed (uscan) of 15mm/s at *y*=45mm: (a) in case of Ti-6Al-4V part, and (b) in case of AISI 316L part

[63]

3.5 Closure

In this chapter, validation of the developed code is considered first with the standard analytical work [81] in order to set the boundary conditions properly. Then laser beam is represented in the code as a volumetric heat source and validated with a published paper [80] in order to proper inclusion of the laser source with the related boundary conditions. In both of the cases, a good agreement is found. Hence, the necessary boundary conditions for the present problem is incorporated in the code and predicted related transport phenomena during the laser welding of dissimilar materials. Preliminary, the melting and solidification behaviour of the materials are predicted for a stationary laser beam; subsequently, a parametric study is carried out with an outcome for the limit to the travelling speed of the laser under different laser powers. Then, the code is extended for development of weld-pool, depth of penetration etc. under different travelling speeds and different laser powers.

References

[80] A Mohan, D Ceglarek, and M. Auinger, Numerical modelling of thermal quantities for improving remote laser welding process capability space with consideration to beam oscillation, *The Int. J. of Advanced Manuf. Tech*, Vol. 123(2022), pp. 761-782

[81] M. Necati Ozisik, Heat Transfer: A Basic Approach, *McGraw-Hill Education*, 1984

Chapter-IV

Conclusion and Future Works

4.1 Conclusion

Since the laser welding involves melting and solidification of the materials using the high density laser energy source. This leads complexity in predicting the transport phenomena. Moreover, all of such phenomena occur in a very short time. In addition, it is found that all weld properties depend on various parameters such as laser power, travelling speed of the laser, positional conditions etc., accordingly the weld bead geometry is formed, leads to the desire properties of the welds. Thus, in order to extend of the laser welding in industrial applications and make such process as more reliable, this work considers the understanding of the process of laser welding in details; and to develop the necessary concepts for its applications.

Joining of dissimilar materials throws a challenge, now-a-days, to the researchers which has wide application in nuclear sectors, space craft industries, petrochemical sectors, automobile sectors, cryogenic industries etc., and on other hand, the demand of laser welding is increasing gradually. This work, thus, considers joining of two dissimilar metals (Ti-6Al-4V titanium alloy and AISI 316L stainless steel) using laser. Since the experimentaion is very expensive, this work considers a numerical work. The numerical study based on the finite volume method (FVM),

involves presenting a suitable mathematical model of melting and solidification (using the mass, momentum and energy equation along with related source terms and enthalpy update scheme) with the laser beam as a volumetric heat source, subsequent consideration of a numerical model using power law scheme, SIMPLER and TDMA algorithms, and development of a code on FORTRAN platform. Hence, it involves validation of the developed code, and subsequent prediction of the results: temperature distribution, area of HAZ, penetration depth, weld-bead geometry under different process parameters.

The validation of the developed code is considered first with a standard analytical work in order to set the boundary conditions properly. Then laser beam is represented in the code as a volumetric heat source and validated with a published paper in order to proper inclusion of the laser source with the related boundary conditions. In both of the cases, a good agreement is found. Hence, the necessary boundary conditions for the present problem is incorporated in the code and predicted related transport phenomena during the laser welding of dissimilar materials. Preliminary, the melting and solidification behaviour of the materials are predicted for a stationary laser beam; subsequently, a parametric study is carried out with an outcome for the limit to the travelling speed of the laser under different laser powers. Then, the code is extended for development of the weld-pool, depth of penetration etc. under different travelling speeds and different laser powers. The major findings are as:

(i) High buoyancy induces in the melt of AISI 316L than Ti-6Al-4V and results flow from AISI 316L part to the Ti-6Al-4V part. Hence, mixing of the materials is possible.

(ii) Size of weld-pool, depth of penetration and HAZ increases with increase of the laser power.

(iii) Size of weld-pool, depth of penetration and HAZ decreases with increase of the travelling speed of the laser beam.

4.2 Scope of the Future Works

(i) All properties of the weld materials are temperature dependent. Variable properties may be incorporated in the numerical code.

(ii) Incorporation of mixing of the weld materials and their transport in the model and subsequent numerical code.

(iii) Incoporation of the non-uiform grids in order to obtain proper shape of the weld-pool, and proper distribution of the temperature, melt-front etc.

(iv) Consideration of volume average properties in the model and numerical code.

(v) Consideration as the binary mixtures of the materials instead of pure/eutectic metal consideration.

(vi) Consideration of the both the thermal and solutal buoyancies.

(vii) Consideration of different models in order to represent the laser beam as a volumetric heat source etc.